# High replication stress and limited Rad51-mediated DNA repair capacity, but not oxidative stress, underlie oligodendrocyte precursor cell radiosensitivity

**N. Daniel Berger[1,2], Peter M. Brownlee[1,3], Myra J. Chen[1,2], Hali Morrison[4], Katalin Osz[1], Nicolas P. Ploquin[4], Jennifer A. Chan[1,2,5,†] and Aaron A. Goodarzi ©[1,3,4,*,†]**

[1]Charbonneau Cancer Institute, University of Calgary, Calgary, Alberta, Canada, [2]Alberta Children's Hospital Research Institute, University of Calgary, Calgary, Alberta, Canada, [3]Department of Biochemistry & Molecular Biology, University of Calgary, Calgary, Alberta, Canada, [4]Department of Oncology and Department of Physics and Astronomy, University of Calgary, Calgary, Alberta, Canada and [5]Department of Pathology & Laboratory Medicine, University of Calgary, Calgary, Alberta, Canada

## ABSTRACT

**Cranial irradiation is part of the standard of care for treating pediatric brain tumors. However, ionizing radiation can trigger serious long-term neurologic sequelae, including oligodendrocyte and brain white matter loss enabling neurocognitive decline in children surviving brain cancer. Oxidative stress-mediated oligodendrocyte precursor cell (OPC) radiosensitivity has been proposed as a possible explanation for this. Here, however, we demonstrate that antioxidants fail to improve OPC viability after irradiation, despite suppressing oxidative stress, suggesting an alternative etiology for OPC radiosensitivity. Using systematic approaches, we find that OPCs have higher irradiation-induced and endogenous γH2AX foci compared to neural stem cells, neurons, astrocytes and mature oligodendrocytes, and these correlate with replication-associated DNA double strand breakage. Furthermore, OPCs are reliant upon ATR kinase and Mre11 nuclease-dependent processes for viability, are more sensitive to drugs increasing replication fork collapse, and display synthetic lethality with PARP inhibitors after irradiation. This suggests an insufficiency for homology-mediated DNA repair in OPCs—a model that is supported by evidence of normal RPA but reduced RAD51 filament formation at resected lesions in irradiated OPCs. We therefore propose a DNA repair-centric mechanism of OPC radiosensitivity, involving chronically-elevated replication stress combined with 'bottlenecks' in RAD51-dependent DNA repair that together reduce radiation resilience.**

## INTRODUCTION

Radiotherapy is an important, effective component of the clinical management of brain tumors; however, it can also cause serious long-term neurologic sequelae, especially in children (1–19). These late effects are characterized by altered white matter development (20), decreases in white matter volume (12), progressive deficits in neurocognitive performance (1,2,7,13,14,18), and a heightened risk of secondary meningiomas or high-grade gliomas arising within the radiotherapy field (8–10,17,21–26). These late effects are prevalent, and two-thirds of children with brain cancer who live longer than 5 years post radiotherapy will experience >1 treatment-related adverse neurologic impact (2). These adverse neurological outcomes are generally more severe the younger a person is treated, and/or with higher cumulative doses of ionizing radiation (IR) (12,13). Lasting neurologic morbidities of brain irradiation can be severe, and understanding their molecular underpinnings is imperative to improving outcomes, particularly in the context of pediatric brain cancer treatment.

Within the brain, there are multiple neural cell types and lineages, including astrocytes and neurons that arise from neural stem progenitor cells (NSPCs), and intermediate and mature oligodendrocytes that arise from proliferative oligodendrocyte precursor cells (OPCs) (27). NSPCs and OPCs are both highly proliferative, whilst neurons, astrocytes and mature oligodendrocytes exist in a post-mitotic, differentiated state. During embryonic and postnatal neural cell differentiation, each lineage has distinct markers and occupies a distinct zone (summarized in Supplementary Figure S1). The majority of cell proliferation occurs within the

---

*To whom correspondence should be addressed. Tel: +1 403 220 4896; Email: a.goodarzi@ucalgary.ca
†The authors wish it to be known that, in their opinion, the last two authors should be regarded as Joint Senior Authors.

ventricular and sub-ventricular zones that are hypersensitive to IR (28) that also shows higher endogenous apoptosis (29), with mature, differentiated cells migrating towards grey and white matter. White matter is comprised largely of neurons with axons protected by myelin sheaths produced by the wrapping processes of mature oligodendrocytes (11,30). As white matter atrophy is a hallmark feature of radiation-related brain injury (3,4,12,16,19) and, as the extent of it correlates with neurocognitive outcomes (2,14,16), there has been particular interest in the sensitivity of the oligodendrocyte lineage to irradiation. Indeed, demyelination and loss of OPCs has been documented in post-mortem human specimens obtained from irradiated patients (31). Both *in vitro* cell-based and *in vivo* animal-based experimental models recapitulate this, and OPCs are now well documented as being radiation sensitive (6,31–35).

Therapeutic IR typically encompasses photon radiation such as x-rays or gamma-rays that exert a large proportion of their anti-tumor effects via reactive oxygen species (ROS) generation and indirect DNA ionization (4,6,19,33,36). Oligodendrocytes are sensitive to ROS in a variety of pathologic settings, including models of hypoxic-ischemic injury (37–40), traumatic brain injury (41), multiple sclerosis (42,43), and Alzheimer's disease (44). Supplementation of animal diets with antioxidants such as edaravone (45), magnesium sulfate (40) or Trolox (46) exhibited a degree of oligodendrocyte rescue in some of these models. That being the case, it is reasonable to hypothesize (and it has been suggested (6)) that the internal oxidative environment of oligodendrocytes and OPCs may contribute to their radiosensitivity. However, there has yet to be a systematic study to verify this hypothesis within the larger context of other neurological lineages, or to explore the molecular mechanisms that underlie OPC's unique radiation sensitivity. In the absence of clear knowledge on this process, meaningful therapeutic interventions to reduce the negative side effects of brain tumor radiotherapy cannot be pursued. Here, we uncover previously undescribed differences in the response of OPCs and other neural cell types to IR exposure, and challenge the notion that OPC radiosensitivity is caused predominantly by elevated oxidative stress. Rather, we present evidence for a DNA replication-associated damage and repair capacity-centric model for OPC-radiosensitivity.

## MATERIALS AND METHODS

### Cell culture

OPC isolation was based on (47). Briefly, anterior cortices of E17 CD-1 mouse pups were dissected, mechanically and enzymatically dissociated with Accumax (EMD Millipore SCR006) and grown in a tri-gas incubator at 37°C and 5% $CO_2$, 5% $O_2$ in low adhesion tissue culture flasks (Sarstedt 83.3911.502) in DMEM consisting of 2% B-27 supplement (Gibco 17504044), 2 mM Glutamax (Gibco 35050061), and 20 ng/ml bFGF (Stemcell 78003.2) and EGF (Stemcell 78006.2) (basal neural precursor media) for 5–7 days. Once small spheres were visible, cells were passaged into $\frac{1}{2}$ conditioned basal neural precursor media and $\frac{1}{2}$ OPC media, DMEM + 2% B27, 2 mM GlutaMAX-I, 20 ng/ml bFGF and 40 ng/ml PDGFaa (Peprotech 100–13A-100ug). Cells

were gradually changed into 100% OPC media by replacing $\frac{1}{2}$ of the existing conditioned media with OPC media over the course of 2 weeks, and resulting oligospheres were enzymatically dissociated into 10 cm tissue culture dishes coated with poly-D-lysine (Millipore Sigma A-003-E) and laminin (Invitrogen 23017015) and allowed to expand to desired confluency. For neural stem cell (NSPC) isolation, the ventricular zone of E12.5 CD-1 mouse brains were dissected out, and tissue was mechanically and enzymatically dissociated with Accumax. Cells were grown in a tri-gas incubator at 37°C and 5% $CO_2$, 5% $O_2$ in NeuroCult proliferation media (Stemcell 05702) supplemented with heparin (Stemcell 07980) and 20 ng/ml bFGF and EGF. When spheres reached 100–200 μm in diameter, they were passaged using Accumax and re-plated in low adhesion tissue culture flasks at 20 000 cells/ml.

### Neural cell lineage differentiation

NSPCs were seeded on poly-D-lysine/laminin coated coverslips or culture vessels for neuronal differentiation, and on Geltrex (ThermoFisher A1413301) coated vessels for astrocyte differentiation, at 25 000 cells/cm² in complete NSPC media. Cells were left to adhere and proliferate for 24 h. For neuronal differentiations, media was then changed to complete neuronal differentiation media for neurons: Neurobasal (Gibco 21103049), 2 mM GlutaMAX-I and 2% B-27+ (Gibco A3582801). For astrocyte differentiation, media was changed to complete astrocyte differentiation media: DMEM, 2 mM GlutaMAX-I, 1% N2 (Gibco 17502048) and 1% FBS (Gibco 16000044). Cells were differentiated for 5–7 days, and $\frac{1}{2}$ of media was refreshed every day for the duration of differentiation until cells were ready for use. Differentiation for OPCs to mature oligodendrocytes (mOLs) was based on (Chen 2007). OPCs were seeded on poly-D-lysine/laminin coated culture vessels at 30 000 cells/cm² in complete OPC media. OPCs were allowed to adhere and proliferate for 24 h, before OPC media was replaced with complete oligodendrocyte media: DMEM, 2 mM GlutaMAX-I, 2% B-27, 15 nM T3 (Millipore Sigma T6397-100MG, prepared as a 15 mM stock in 0.1 M NaOH, diluted to 1000 × 15 μM T3 in DMEM), 30 μM *N*-acetyl-L-cysteine (Millipore Sigma A7250-10G, prepared as a 1000 × 30 mM stock in DMEM, pH adjusted to 7.4), and 10 ng/ml CNTF (Stemcell 78010.1). Base oligodendrocyte media consisted of DMEM, 2 mM GlutaMAX-I and 2% B-27, and each day, $\frac{1}{2}$ of mOL media was refreshed with complete mOL media with fresh T3, NAC and CNTF added to the base mOL media at the time of use. Cells were differentiated for 5–7 days at 5% $O_2$.

### Cell irradiation

For X-ray photon irradiation experiments, cells were plated in Cellvis no. 1.5 glass bottom plates (Cellvis P9601.5H-N). 96-well plates were irradiated via a Varian TrueBeam Linear Accelerator (LINAC). A planning CT scan was acquired to delineate the irradiation volume and calculate the dose to be delivered to a 96-well plate with 200 μl liquid in each well. A custom fit heat moulded plastic jig was fabricated

to provide full lateral photon scatter conditions to the 96-well plate. 5 cm of Solid Water High Equivalency (Standard Imaging) slabs were placed under the 96-well plate to provide full backscatter conditions and 2 cm above it to provide full charged particle equilibrium conditions. The radiation plan was created to deliver the radiation dose homogeneously ($\pm 5\%$) over the 96-well plates. Using the lasers and crosshairs of the LINAC, the 96-well plate was aligned with the treatment couch and gantry in a reproducible, consistent manner. As per the treatment plan, a field size of $X = 15$ cm and $Y = 10$ cm was used, with a Source to Surface Distance (SSD) of 96-cm to the top of the solid water. 2.4 Gy (or a calculated 49.6 MU) of 6 MV X-rays were delivered with a dose rate of 300 MU/min on the Varian LINAC. For $\gamma$ ray irradiations, cells were irradiated using a GammaCell 1000 Elite source (MDS Nordion), which contains a $^{137}$Cs source that emits approximately 2.9 Gy/min.

### Immunofluorescence microscopy

Cultured OPCs were treated with $1\times$ trypsin-EDTA (10X, Millipore Sigma 594180-100ML) in pre-warmed PBS to facilitate removal from 10 cm dishes, centrifuged at 1500 rpm for 3 min, gently resuspended in pre-warmed complete OPC media and counted. NSPCs were centrifuged at 1500 rpm for 3 min, resuspended in Accumax for 5 min at 37°C for neurosphere dissociation, gently resuspended in complete NSPC media and counted. Cells were plated on poly-D-lysine (1 h, 37°C) and laminin (overnight, 37°C) coated 18 mm coverslips (Mandel, NEU-GG-18-pre) at 100 000 cells/coverslip and allowed to expand overnight. After treatment with IR or drug, cells were fixed for 10 min in 4% PFA/PBS (ThermoScientific AAJ19943K2) then rinsed in $1\times$ PBS. Permeabilization was performed with $1\times$ PBS + 0.25% Triton X-100 (Millipore Sigma T8787-250ML) for 3 min at room temperature (RT). Cells were rinsed with $1\times$ PBS and blocked for 30 min with 3% goat or horse serum in PBST ($1\times$ PBS + 0.1% Tween 20 (Millipore Sigma P1379-500ML)). Primary antibodies applied for 1 h at RT in 1% serum/PBST. Alexa Fluor secondary antibodies were applied at 1:1000 dilution for 25 h RT. Nuclei were counterstained in a 1:10 000 dilution of 1 mg/ml 4′,6-diamidino-2-phenylindole (DAPI; Millipore Sigma D9542-10MG) and mounted with FluorSave Reagent (Calbiochem 34578920ML).

### Antibodies and reagents

Primary antibodies were Nestin (1:200, Millipore Sigma, MAB353), Sox2 (1:200, Cell Signaling Technology #3728S), Olig2 (1:500, Abcam ab109186), PDGFRα (1:200, Cell Signaling Technology #3174S), NG2 (1:500, Millipore Sigma AB5320), O4 (1:200, Millipore Sigma MAB345), MBP (1:200, Abcam ab40390), GFAP (1:800, Millipore Sigma AB5541), γH2AX (1:800, Abcam ab26350), RPA$^{2S33P}$ (1:1000, Abcam ab211877), RAD51 (1:1000, Abcam ab133534), B-III tubulin (1:500, R&D Systems MAB1195), H3$^{S10P}$ (1:500, Abcam ab14955). Reagents and inhibitors ATMi (KU55933) used at 10 μM (Tocris, #3544), DNA-PKi (NU7441) used at 1 μM (Selleckchem #S2638), MRE11i (Mirin) used at 25 μM

(Selleckchem #S8096), PARPi (AZD2289) used at 0.01 μM (Selleckchem #S1060), ATRi (AZD6738) used at 0.5 μM (Cayman Chemicals #21053), hydroxyurea used at 0.5 mM (Millipore Sigma H8627-5G), methyl methansulfonate used at 100 μM (Millipore Sigma #129925-5G), thiotepa used at 10 μM (Selleckchem #S1775), etoposide used at 0.1 μM (Millipore Sigma E1383-25mg), camptothecin used at 1 μM (Selleckchem #S1288), cisplatin used at 1 μM (Millipore Sigma P4393-100MG), trolox used at 10 μM (Millipore Sigma #238813-1G), edaravone used at 10 μM (Selleckchem S1326), N-acetyl-L-cysteine used at 30 μM (Millipore Sigma A7250-10G), glutathione used at 10 μM (Millipore Sigma G4251-300 MG), and EdU used at 10 μM (ThermoFisher C10339).

### Microscopy image acquisition and processing

Images were acquired on a Zeiss LSM 880 Confocal Microscope with Airyscan, and processed for false colorization, overlay/colocalization, orientation and scale with Zeiss Zen Lite. Enumeration of RAD51 and γ2AX foci was performed manually by counting cells using Adobe Photoshop CC 18. Enumeration of cells for nuclear, cytoskeletal, cytoplasmic and membrane proteins was also performed manually with Adobe Photoshop CC18. Nuclear quantification of γ2AX and RPA2$^{S33p}$ was performed with FIJI version 2.0.0. Briefly, 16 bit greyscale DAPI images were processed with Gaussian blur and auto-thresholded with Default. Images were converted to binary masks and the watershed tool was run to separate nuclei further. Nuclear masks were used to quantify the immunofluorescence signal of the stain of interest via the 'analyze particles' function, and integrated density provided fluorescence intensity values. For γ-H2AX, RAD51 and RPA2$^{S33p}$ automated foci counting analyses, maximum intensity projections from z-stacked images were analyzed using CellProfiler (BROAD Institute). Briefly, the Speckle Counting pipeline was used to count the number of γ-H2AX, RAD51 or RPA2$^{S33p}$ foci per nucleus using the DAPI stain as a mask. Foci were automatically identified using a single intensity threshold that was established and used across all images sets for each antibody stain.

### Alamar Blue cell viability assay

To assess cell viability after radiation or treatment with small molecules, Alamar Blue resazurin-based cell viability reagent (Invitrogen DAL1100) was added to cell culture media to a final concentration of 10% in media 16 h after IR or treatment with small molecules. Twenty-four hours later, the resulting fluorescence was read on a Molecular Devices SpectraMax iD3 microplate reader with excitation filters set at 530 nm and emission at 580 nm. For each experiment, the fluorescence from no less than three wells were averaged together per condition, and negative (no cell) controls were used to determine background media fluorescence.

### 2D propidium iodide and EdU flow cytometry

For flow cytometry analyses, NSPCs and OPCs were seeded in poly-D-lysine/plaminin coated 6-cm dishes (Greiner Bio-One 628160) at 800 000 cells per vessel in complete NSPC

or OPC media, and allowed to adhere and proliferate for 48 h to 90% confluency. Each repeat was performed in duplicate, and two 6-cm dishes were seeded per condition. EdU (ThermoFisher C10337) or DMSO vehicle control was added to the culture media to a final concentration of 10 μM, and cells were immediately irradiated with 0.5 Gy γ IR. Both irradiated and unirradiated cells were incubated for a further 4 h at 5% $O_2$, before being rinsed twice with 1× ice cold PBS, and collected into 1 ml cold PBS. Cells were centrifuged at 1500 rpm for 3 min, and resuspended in 200 μl ice cold PBS. 800 μl ice cold 100% EtOH was added drop-wise to cells while vortexing slowly, and cells were fixed on ice for a 1 h. If cells were not used immediately, they were kept in the dark at 4°C. For EdU staining, fixed cells were centrifuged at 2500 rpm for 5 min, and washed once with ice cold PBS, centrifuging at 2500 rpm for 5 min again. Cells were resuspended in 100 μl of Click-iT EdU Alexa Fluor 488, or 100 μl of PBS for unstained controls, and stained for 30 min in the dark. Cells were washed twice with ice cold PBS, centrifuging at 2500 rpm for 5 min between each wash, and resuspended in either PBS for unstained controls, or propidium iodide (Abcam 139418). Cells were then run on a BD Bioscience LSRII Flow Cytometer, gating sequentially for cellular debris and doublets as per standard forward and side scattering gating procedures, and single color/unstained controls were used to set thresholds for fluorescence. EdU and PI fluorescence intensities were then examined, and data were analyzed with FACSDiva version 6.1.3. Full details of FACS experiment can be accessed via https://flowrepository.org/ using experiment ID: FR-FCM-Z527

### H2DCFDA reactive oxygen species detection assay

H2DCFDA (ThermoFisher, D399-100mg) was prepared as a stock at 20 mM in DMSO. H2DCFDA was diluted to 40 μM in NSPC or OPC complete media, and 100 μl was diluted 1:1 into 100 μl of media with cells in a 96-well plate for a final concentration of 20 μM. Cells were returned to 37°C at 3% $O_2$ incubation for 1 h to load the dye. If antioxidants were added, they were added concurrently for a 1 h incubation. For IR experiments, plates were irradiated on a Varian TrueBeam LINAC. Immediately prior to irradiation, media was removed and replaced with 200 μl cold PBS (to avoid media autofluorescence at later microplate reading step). Plates were irradiated, and resulting DCF fluorescence was read immediately on a Molecular Devices SpectraMax iD3 microplate reader with filters set for an excitation of 485 nm and emission of 530 nm. For $H_2O_2$ experiments, various concentrations of $H_2O_2$ were diluted into cold PBS, and media was replaced with $H_2O_2$ in cold PBS for 5 min at room temperature. The resulting fluorescence was read as above. For each experiment, the fluorescence values of no less than three wells were averaged together, and no H2DCFDA, unirradiated and vehicle-treated controls were performed with each experiment.

### Alkaline comet assay

NSPCs and OPCs were grown to 90% confluency (∼5 million cells) in poly-D-lysine and laminin coated 10 cm dishes,

and were trypsinized, collected, counted and resuspended to 1000 cells/ml in ice cold 1× HBSS without calcium or magnesium in 15 ml Falcon tubes and kept on ice (Fisher Scientific 14025076). 1 ml cells were removed prior to irradiation for unirradiated controls, and cells were irradiated with 0.5, 3 or 10 Gy γ IR and immediately, 1 ml was removed for the induction time point. Cells were spin down at 1500 rpm for 3 min before being returned to warm, conditioned and clarified media for repair. 1 h later, 1 ml of cells were removed as the final time point. Cells were washed in pre-chilled 1X PBS, spun down at 1500 rpm for 3 min and resuspended in 150 μl of cold 1× PBS. Cells were mixed with an equal volume of 1.2% (w/v) low melting point agarose (Invitrogen, #16520–050), and quickly layered onto a pre-chilled frosted glass slide with a 0.8% (w/v) ultrapure agarose (Techologist Choice #7109) base layer. Coverslips were used to maintain the agarose shape, and slides were chilled at 4°C in the dark until set. Coverslips were removed, and slides were immersed in pre-chilled lysis buffer (2.5 M NaCl, 10 mM Tris–HCl, 100 mM EDTA, 1% (v/v) Triton X-100, 10% (v/v) DMSO, pH 10) for 1 h in the dark, then washed three times with pre-chilled electrophoresis buffer (50 mM NaOH, 1 mM EDTA, 10% (v/v) DMSO). Slides were placed in electrophoresis chamber with buffer, and allowed to equilibrate for 45 min before being electrophoresed at 25 V for 25 min (0.6 V/cm), and neutralized with Tris–HCl pH 7.4 for 1 h at 4°C. DNA was stained with SYBR Green (1:10,000 from Sigma #S9430) and 0.5% antifade ( = 0.5% (w/v) *p*-phenylenediamine in 20 mM Tris, pH 8.8, 90% (v/v) glycerol) for 10 min at room temperature. Slides were imaged and Comet Assay IV (Perceptive Instruments, UK) software was used to quantify tail moment for at least 100 cells per experiment.

### Quantitative PCR

NSPC and OPC cell pellets were lysed with Trizol reagent (Ambion) to extract RNA. cDNA was synthesized from 1 μg RNA using Superscript II reverse transcriptase (Invitrogen). qPCR analysis was performed using SYBR green (Life Technologies) to determine target gene mRNA expression. Reactions were performed in technical triplicate and CT values were averaged and normalized to the corresponding GAPDH value to obtain the $\Delta$CT value. $\Delta\Delta$CT values were obtained by normalizing the $\Delta$CT values to the NSC cell type and expressed as fold change in expression averaged over three independent repeats. The following primers were used:

- RAD51, Forward: 5′-TGATGAGTTTGGTGTCGCAGTG
- RAD51, Reverse: 5′-CGAACATGGCTGCTCCATCTAC
- RAD52, Forward: 5′-GAGAACCAGCCCAAACTTCTGC
- RAD52, Reverse: 5′-GAACATGCTGGTTGGTGTTGC
- BRCA1, Forward: 5′-CCCAAAGATGAGCTGGAGAG
- BRCA1, Reverse: 5′-GTCCCACATCACAAGACGTG
- BRCA2, Forward: 5′-CCATTTCAGAAGACCAGTGG
- BRCA2, Reverse: 5′-ACGAACACCTATGAGTAGCC
- OLIG2, Forward: 5′-GAAGCAGATGACTGAGCCCGAG
- OLIG2, Reverse: 5′-CCCGTAGATCTGCTCACCAG
- PDGFRA, Forward: 5′-GGAGAACCTGTTGCCGGGG AC

- PDGFRA, Reverse: 5′-TCTCGATGGCACTCTCTTCC
- GAPDH, Forward: 5′-CTCCACTCACGGCAAATTCAA
- GAPDH, Reverse: 5′-GATGACAAGCTTCCCATTCTCG

### Statistics

Statistical analyses were performed using GraphPad Prism 8. Each column represents the mean ± SEM and is representative of at least three independent experimental repeats. Dots in dot plots represent values of single cells, and the mean ± SEM of at least three independent experimental repeats is shown. Data were evaluated by one-way or two-way analysis of variance (ANOVA) followed by the Tukey's test, or alternatively a two-tailed Student's *t*-test. A value of $P < 0.05$ was considered significant. For all figures in this study, the following nomenclature was used to describe statistical significance: ns $P > 0.05$, * $P < 0.05$, ** $P < 0.01$, *** $P < 0.001$ and **** $P < 0.0001$.

### Research Ethics Board approval

Animal use was approved by the University of Calgary Animal Care Committee (protocol AC17-0235) in compliance with the Guidelines of the Canadian Council of Animal Care.

## RESULTS

### Oligodendrocyte Precursor Cells are radiosensitive relative to other neural cell types, and die by apoptosis

To establish a robust model amenable to systematic analysis, we first isolated mouse embryonic NSPCs (E12.5) and OPCs (E17) from wildtype, outbred CD-1 mice that are an established model for brain and radiation research (38,48,49), and differentiated these *ex vivo* into the main neural cell types (27) outlined in Figure 1A. In this system, the cultures antigenically and morphologically recapitulated their *in vivo* counterparts when examined by immunofluorescence (for further rationale for using this model system, please see Supplemental Information). To verify the relative radiosensitivity of different neural cell types in our system, we exposed the cells to IR and used Alamar Blue assays as a surrogate for monitoring cell viability, as well as immunofluorescence staining and cell enumeration to evaluate overall cell population numbers. Individual cultures were exposed to 3 Gy IR, and viable cells expressing lineage-specific markers were enumerated 24 h later and expressed as a surviving fraction relative to the 0 Gy condition (Figure 1B). As expected (6,29–33), OPCs displayed the greatest radiosensitivity relative to other neural cell types. To examine cell death mechanisms, cleaved Caspase 3 (an indicator of apoptosis) (33) was measured 6 h post 3 Gy IR (Figure 1C). Astrocytes, neurons, mOLs and NSPCs showed modest increases in cleaved Caspase 3 after IR, none of which were significant ($P > 0.05$) relative to controls or one another. By contrast, OPCs showed a significant ($P < 0.0001$) 7.32-fold increase in programmed cell death after IR. As increased radiosensitivity can be a consequence of proliferation at the time of irradiation, we also performed a 0.25–20 Gy IR dose course using NSPCs and OPCs that were

in a comparably proliferative state (Figure 1D). Proliferating OPCs displayed significant ($P < 0.0001$) radiosensitivity relative to proliferating NSPCs even at low IR doses, suggesting that OPC radiosensitivity is not solely a function of cell division at the time of irradiation. We noted that the lower threshold of sensitivity of this viability assay (i.e. the signal produced from dead cultures) was 10–20%. For example, OPC cultures 24 h after 3 or 20 Gy IR (as in Figure 1D) were visibly dead (Supplemental Figure S2) but generated an average ∼20% Alamar Blue signal in that experiment. To indicate this on all viability assays in this study, the 'lower limit of sensitivity (all dead)' threshold level (verified for that specific experiment) was applied to datasets.

### OPC radiosensitivity is not alleviated by oxidative stress suppression

To interrogate the hypothesis that elevated oxidative stress underlies OPC radiosensitivity, we monitored oxidative stress using the 2′,7′-dichlorofluorescin diacetate ($H_2DCFDA$) assay in cells exposed to IR or $H_2O_2$ (as a positive control for oxidative stress), as we have done before (50). $H_2DCFDA$ freely permeates cells and reacts with ROS in a stoichiometric manner to produce fluorescent dichlorofluorescin (DCF). OPC and NSPC cultures were pre-incubated with $H_2DCFDA$ for 1 h, irradiated or exposed to $H_2O_2$, and DCF fluorescence was measured immediately by microplate reader. Compared to NSPCs, OPCs displayed greater oxidative stress at baseline and post-IR or $H_2O_2$ treatment (Figures 1E, F). We next exposed OPC and NSPC cells to a series of individual and mixed antioxidants, and verified that treatments effectively suppressed oxidative stress (Figures 1E, F and Supplementary Figure S3A, B). To determine whether higher OPC oxidative stress was responsible for their heightened sensitivity to IR, OPCs and NSPCs with a comparable proliferative index were treated with antioxidants for 24 h, irradiated, and assessed for viability 16 h later. While no effects were observed in NSPCs (expected given their low oxidative stress and high viability), surprisingly, the suppression of oxidative stress to background levels had no effect on OPC viability after IR exposure (Figure 1G and Supplementary Figure S3C). Altogether, these data suggest that elevated oxidative stress does not underlie OPC radiosensitivity.

### OPCs display high basal and IR-induced DNA damage burden

We considered alternative explanations for OPC radiosensitivity, and explored whether these cells exhibited any aberrant DNA damage responses. As we have done previously (50), we used using alkaline comet assays to directly measure induction and resolution of DNA single strand breaks (SSBs) and, to a lesser extent, DNA double strand breaks (DSBs). OPCs and NSPCs were exposed to 3 or 10 Gy R, and then subjected to single-cell gel electrophoresis (Figure 2A). OPCs displayed significantly ($P < 0.0001$) increased DSB and SSB levels at baseline and after both doses of IR compared to NSPCs. We also monitored the baseline presence, induction and resolution of γH2AX (H2AX[S139p]) foci
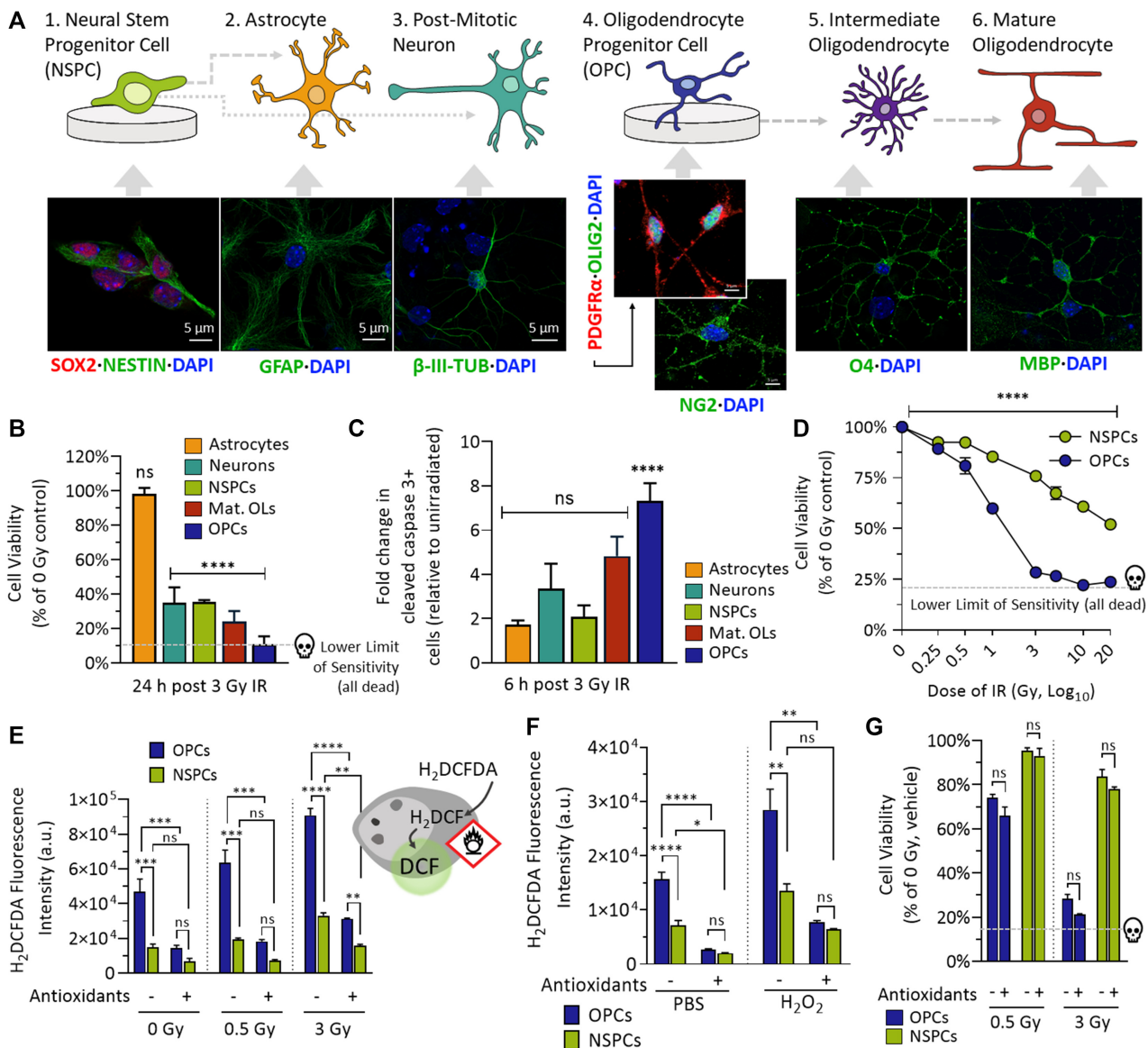
**Figure 1.** Oligodendrocyte Progenitor Cell radiosensitivity cannot be alleviated by oxidative stress suppression. Panel A. Mammalian brain (neural) cells of OPC or NSPC-derived lineage are distinguished by immunofluorescence using the indicated markers. Panel B. NSPCs or OPCs were differentiated into individual neural cell lineages as in (**A**), exposed to 3 Gy IR, and monitored 24 h later for viability. Dashed grey lines and skull icon represents the specific lower limit of sensitivity for this Alamar Blue assay (the point at which all cells in the culture are dead). Panel C. Neural cells were irradiated with 3 Gy IR, then, 24 h later, immuno-stained for cleaved caspase 3, and quantified within each distinct neural lineage as a function of total cell number. To yield an apoptotic index, irradiated cells were normalized to 0 Gy condition. Data = mean ± SEM of $n = 3$ with 500–1000 cells per biologic replicate. Panel D. NSPC (green) and OPC (blue) cultures were irradiated with increasing IR doses and monitored for viability. Data = mean ± SEM of $n = 3$. Lower limit of sensitivity is indicated as in (**B**). Panel E. The inset schematic depicts the basis of the DCF oxidative stress assay. NSPC (green) and OPC (blue) cultures were pre-treated with or without the comprehensive antioxidant cocktail prior to 0.5 or 3 Gy IR, then monitored immediately using the DCF fluorescence oxidative stress assay. Data = mean ± SEM of n = 3. Panel F. The experiment from (**E**) was repeated using a 5 min incubation with 500 μM $H_2O_2$ treatment (or PBS alone) prior to analysis. Panel G. NSPC (green) and OPC (blue) cultures were pre-treated with an antioxidant mixture and exposed to a single dose of 0.5 or 3 Gy X-IR, and assessed for viability as in (**B**). Data = mean ± SEM of $n = 4$. For data in (**B, C, G**), statistical analysis represents pairwise comparisons analyzed with Student's *t*-test. Data in (**D**) was analyzed with a two-way ANOVA. Data in (**E–G**) was analyzed by one-way ANOVA with Tukey's multiple comparison post-test. For all panels, ns $P > 0.05$, * $P < 0.05$, ** $P < 0.01$, *** $P < 0.001$, ****$P < 0.0001$. Icons and graphics in figure were created using Adobe Illustrator, or Microsoft PowerPoint.
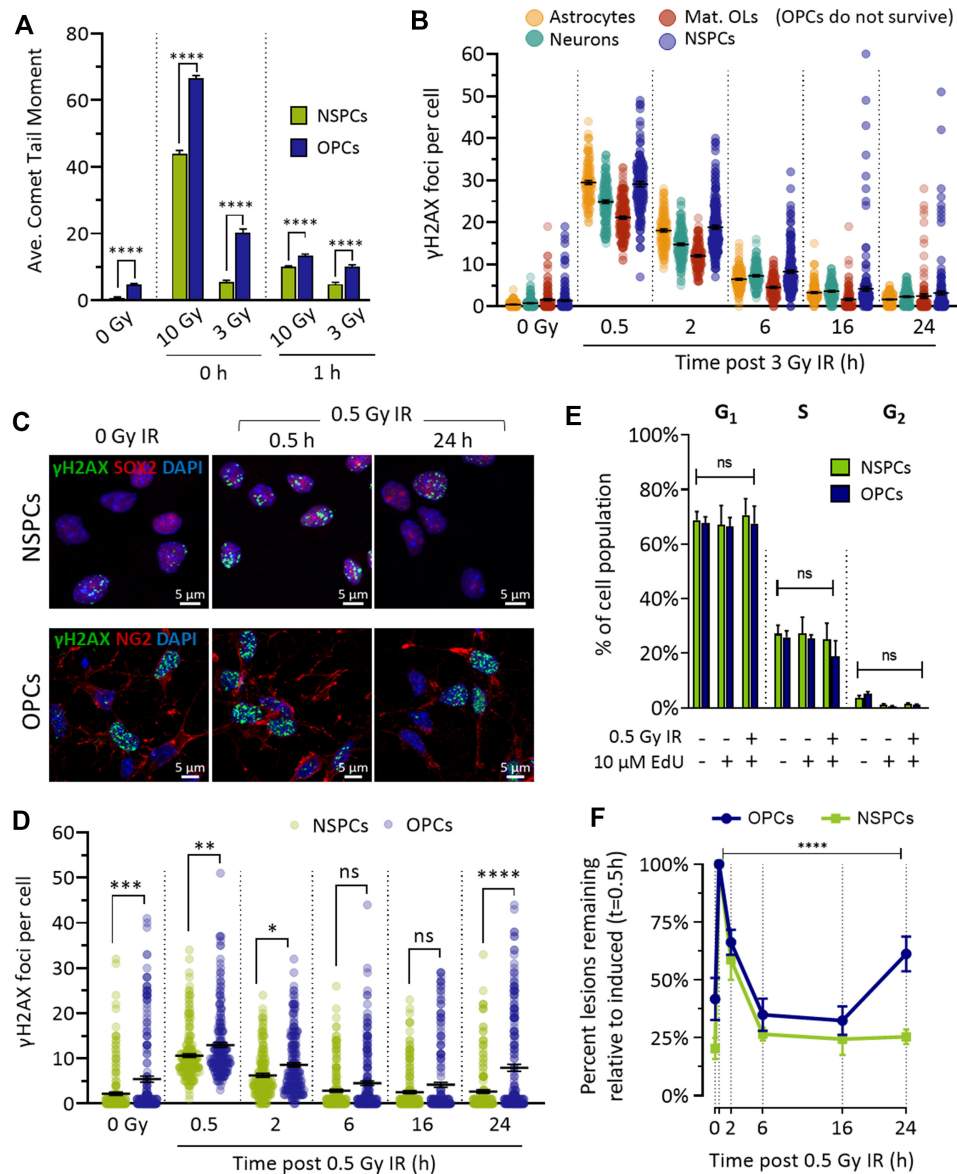
**Figure 2.** OPCs experience a high baseline and IR-induced DNA damage burden. (**A**) OPCs and NSPCs were irradiated with 3 or 10 Gy IR and, either immediately (0 h) or 1 h later, subjected to alkaline single cell gel electrophoresis (comet assay) to examine DNA double strand and single strand break induction and resolution. Tail moments were captured using Comet Assay IV software. Data = mean ± SEM of $n = 3$ with 200 cells per repeat. Data were analyzed by one-way ANOVA with a Tukey's multiple comparisons post-test. (**B**) Astrocytes, Neurons, Mature Oligodendrocytes and NSPCs were exposed to 3 Gy and, from 0.5 to 24 h later, fixed and immunostained for γH2AX, Individual γH2AX foci were enumerated and expressed as dot plots of foci per cell, with black bars = mean ± SEM from $n = 3$ with 50–80 cells per repeat. Pairwise comparisons were analyzed with Student's t-test; note that OPCs exposed to 3 Gy did not survive long enough to obtain reliable data. (**C**) Asynchronously growing cultures of NSPCs and OPCs were irradiated with 0.5 Gy IR and immunostained 0.5 or 24 h later for γH2AX (green), DAPI (blue) and the indicated neural lineage markers (red). (**D**) Individual γH2AX foci were enumerated for the NSPCs (green) and OPCs (blue) from (C); dot plot represents foci per cell, with black bars = mean ± SEM from $n = 3$ with 50–80 cells per repeat. Pairwise comparisons were analyzed with Student's t-test. (**E**) Cells from (C, D) were pulsed with 0.5 μM EdU ± 0.5 Gy IR and distribution of G1, S, G2 phase populations were quantified using FACS. Panel F. Data from (D) was normalized to the 0.5 h time point ('induced') to monitor the rate of γH2AX signal resolution between NSPCs (green) and OPCs (blue). For all panels, ns $P > 0.05$, * $P < 0.05$, ** $P < 0.01$, ***$P < 0.001$, **** $P < 0.0001$.

(a highly sensitive, surrogate marker of DSBs) after IR in a cell type-specific manner (51) (Figure 2B). Proliferative NSPCs displayed increased γH2AX after 3 Gy IR compared to non-proliferative neural cell types, although this still resolved over time. 3 Gy IR triggered too much cell death in OPCs to obtain reliable data. To solve this, we repeated this experiment using a sub-lethal dose (0.5 Gy)

that permits OPCs to survive at least 24 h (Figure 1D) and monitored γH2AX in OPCs and NSPCs with comparable proliferative and cell cycle profiles (Figure 2C–E). OPCs showed greater γH2AX at all timepoints examined. Normalizing γH2AX signal to the peak of induction (at 0.5 h) showed that overall γH2AX resolution kinetics of OPCs and NSPCs was similar over the first 6 h, arguing against
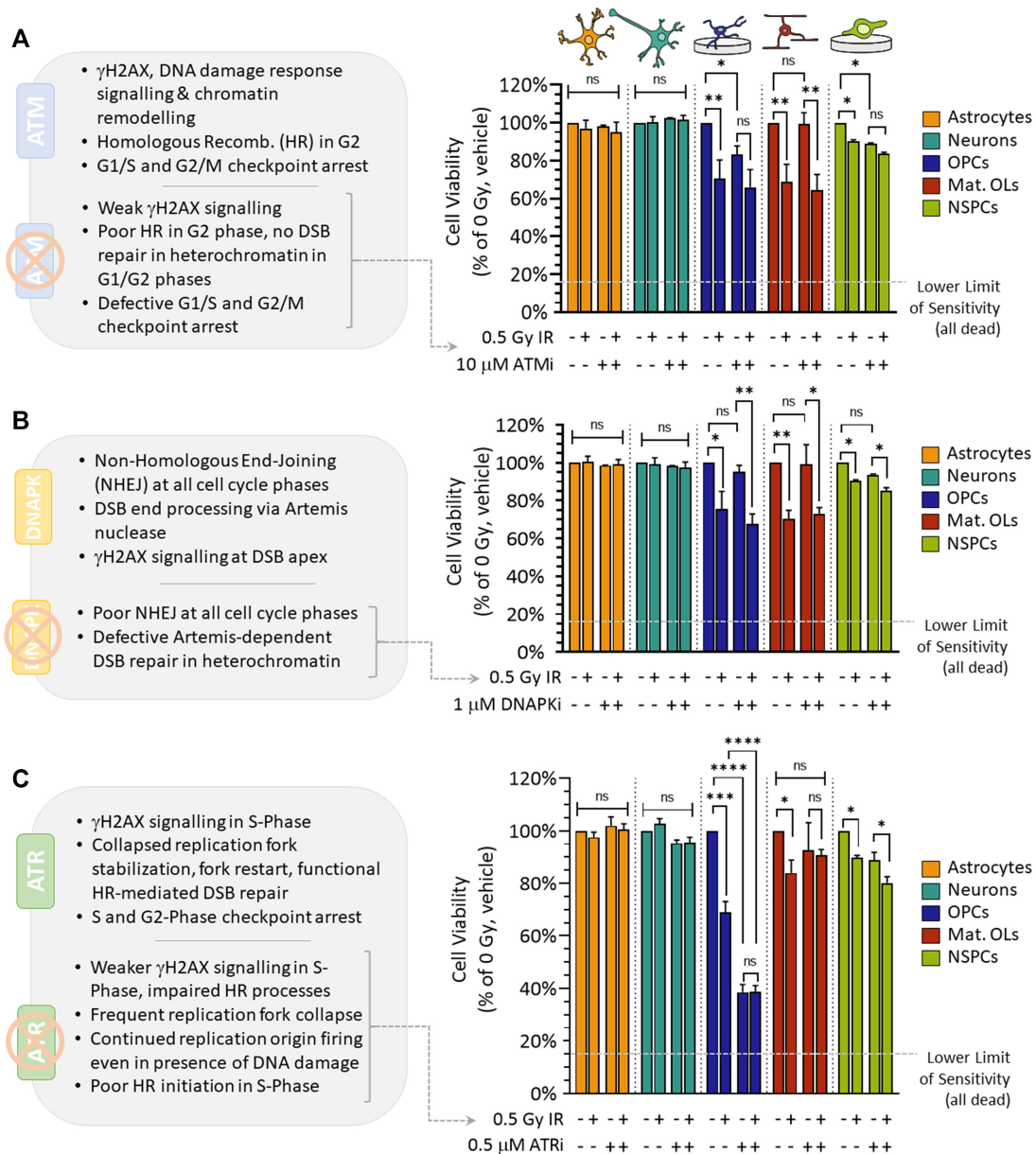
**Figure 3.** OPCs are highly dependent upon ATR for survival. Left hand insets in all panels summarize the impact of drug treatment on cells. (**A**) Individual neural cell lineages were incubated with 10 μM of the ATM inhibitor KU55933 (or an equivalent amount of the DMSO vehicle) for 1 h, then exposed to 0.5 Gy IR and monitored 40 h later for viability using microplate reader. (**B**) The experiment in (A) was repeated using 1 μM of the DNA-PK inhibitor NU7441 (or an equivalent amount of the DMSO vehicle). Bars represent mean ± SEM of $n = 3$ normalized to 0 Gy, DMSO-treated controls. (**C**) The experiment in (A) was repeated using 0.5 μM of the ATR inhibitor AZD-6738 (or an equivalent amount of the DMSO vehicle). Bars represent mean ± SEM of $n = 3$ normalized to 0 Gy, DMSO-treated controls. Data in were analyzed with one-way ANOVAs amongst each neural cell type, and a Dunnett's multiple comparisons post-test compared each mean to the unirradiated, untreated control values. For all panels, ns $P > 0.05$, *$P < 0.05$, **$P < 0.01$, *** $P < 0.001$ and ****$P < 0.0001$. Dashed grey lines represent the specific lower limit of sensitivity for this Alamar Blue assay (the point at which all cells in the culture are dead). Graphics in this figure were created using Adobe Illustrator or Powerpoint.

a large, intrinsic DSB repair defect in these asynchronously replicating cell cultures (Figure 2F). From 16 to 24 h, however, OPCs showed an increase in γH2AX not observed in unirradiated OPCs, or in NSPCs under any condition. We speculate that this could be due to irradiated OPC cells re-entering S-phase with unresolved DNA lesions that collide with replication forks to produce further, late-occurring DSBs.

### OPCs depend upon ATR protein kinase activity for survival

The mammalian response to IR involves signaling from the ATM, DNAPK and ATR kinases, which (depending on cell cycle phase) variably contribute to γH2AX signaling, G1/S, intra-S and G2/M cell cycle checkpoint arrest, the initiation of homologous recombination (HR)-mediated DSB repair, replication fork stabilization and/or non-homologous end-joining (NHEJ) mediated DSB repair
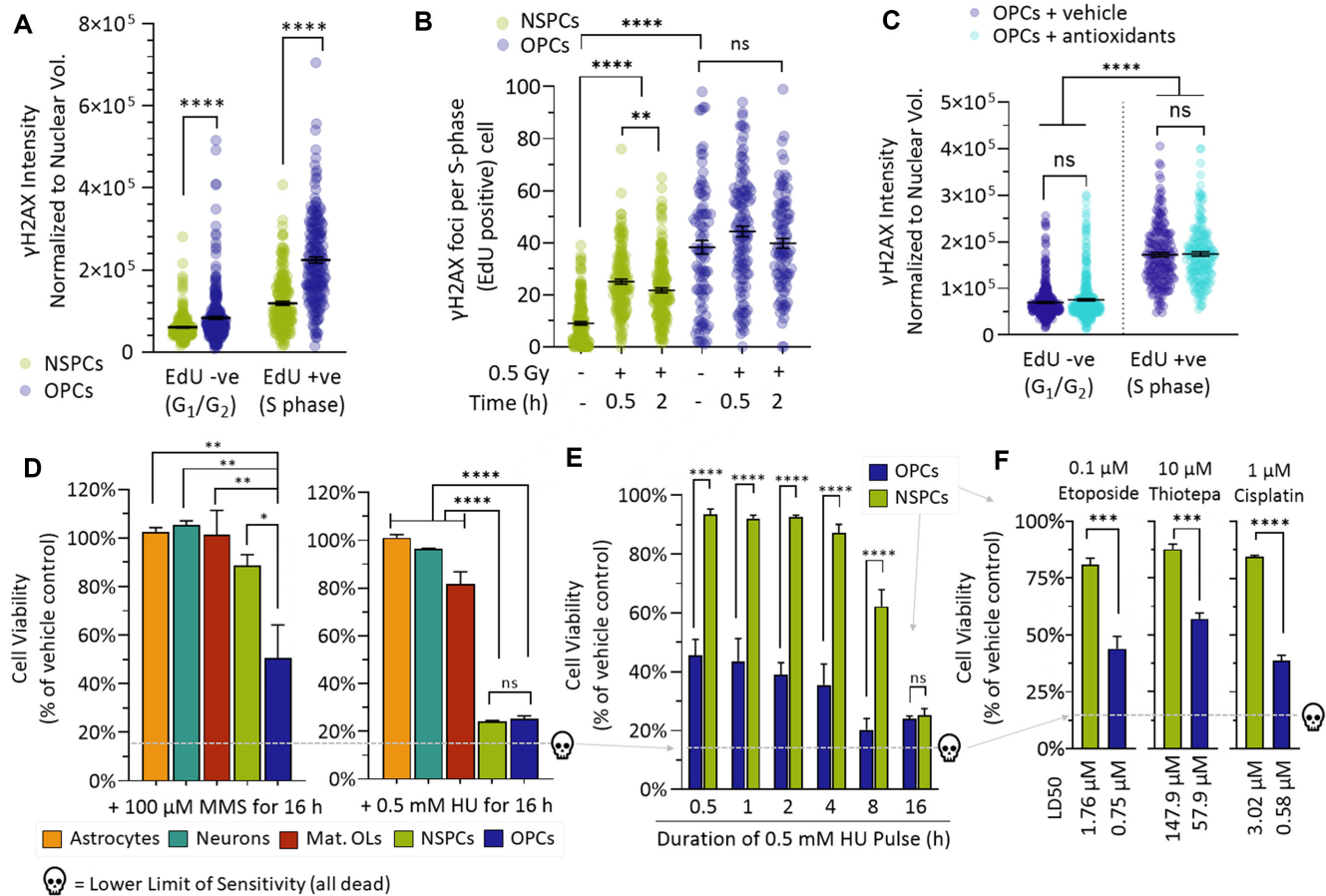
**Figure 4.** OPCs carry a high burden of anti-oxidant insensitive but DNA replication-associated DNA damage and are are sensitive to replication fork collapse. (**A**) Asynchronously growing cultures of NSPCs (green) and OPCs (blue) were pulsed with EdU for 1 h, then immunostained for EdU and γH2AX. Total nuclear γH2AX fluorescence intensity was normalized to total nuclear volume, and then plotted for EdU positive (S-Phase, actively replicating) or EdU negative ($G_1/G_2$, non-replicating) cells. (**B**) The cells from (A) were irradiated with 0.5 Gy and harvested at indicated time points, immunostained for EdU and γH2AX. The number of nuclear γH2AX foci in EdU positive (S-phase) cells was enumerated. (**C**) The comprehensive antioxidant cocktail (cyan) or an equivalent amount of vehicle (dark blue) was added to OPC cultures and, 24 h later, cells were pulsed for 1 h with EdU before being stained for EdU and γH2AX and analyzed as in (A). (**D**) NSPCs or OPCs were cultured and differentiated into individual (indicated) neural cell lineages, which were then incubated with 100 μM methyl methanesulfonate (MMS, left) or 0.5 mM hydroxyurea (HU, right) for 16 h, then washed, placed into fresh media, and assessed for cell viability after an additional 24 h. (**E**) The experiment in (C) was repeated using between 0.5 to 16 h exposure to HU and only NSPC and OPC cell cultures. (**F**) The experiment in (C) was repeated using either etoposide, thiotepa or cisplatin (at indicated doses) for 16 h exposure, and only NSPC and OPC cell cultures. For panels A, B and F, black bars = mean ± SEM of $n = 3$ with 60–100 cells per repeat. Pairwise comparisons were made with Student's *t*-test. For panels C–E, bars represent the mean ± SEM of $n = 3$. Data was analyzed by one-way ANOVA followed by Tukey's multiple comparisons post-test. For all panels, ns $P > 0.05$, *$P < 0.05$, **$P < 0.01$, *** $P < 0.001$ and ****$P < 0.0001$. For panels D–F, dashed grey lines and skull icon represents the specific lower limit of sensitivity for this Alamar Blue assay (the point at which all cells in the culture are dead). Icons in this figure were from Powerpoint.

(see left insets, Figures 3A–C) (52–59). To dissect the relative important of each signaling pathway to neural cell resilience after IR, individual neural cell lineages were incubated with small molecule inhibitors of ATM (Figure 3A), DNAPK (Figure 3B) or ATR (Figure 3C) at concentrations that we verified to produce the established functional outcomes of selective loss of each protein kinase activity (Supplementary Figure S4A–D) before being irradiated with 0.5 Gy. NSPCs were only weakly impacted by IR or loss of ATM, DNAPK or ATR activity, whilst post-mitotic astrocytes and neurons were not impacted at all. Combined loss of ATM or ATR with IR had a small additive impact on NSPC viability, fitting with the fact that these are proliferative cells that will utilize ATM/ATR-dependent checkpoint arrest and/or S and G2-phase specific repair pathways (such as HR) after exposure to IR. Compared to the NSPC lineage, OPC and mOL viability was more impacted by 0.5 Gy IR, fitting with earlier results (Figure 1B–D). Loss of DNA-PK activity did not impact mOL or OPC radiosensitivity, suggesting that NHEJ-mediated DSB repair is dispensable for their viability. mOLs were also unaffected by ATM or ATR inhibition, whether irradiated or not, most likely reflecting their post-mitotic state and thus no need for cell cycle arrest pathways or S/G2-phase specific repair pathways. By contrast, OPC viability was negatively impacted by inhibition of ATM (to a small extent) and ATR (to a large extent), with epistasis between 0.5 Gy IR and inhibitors in both cases. The relatively large impact of ATR loss on OPC viability suggests a strong reliance upon S/G2-phase specific DNA damage responses.
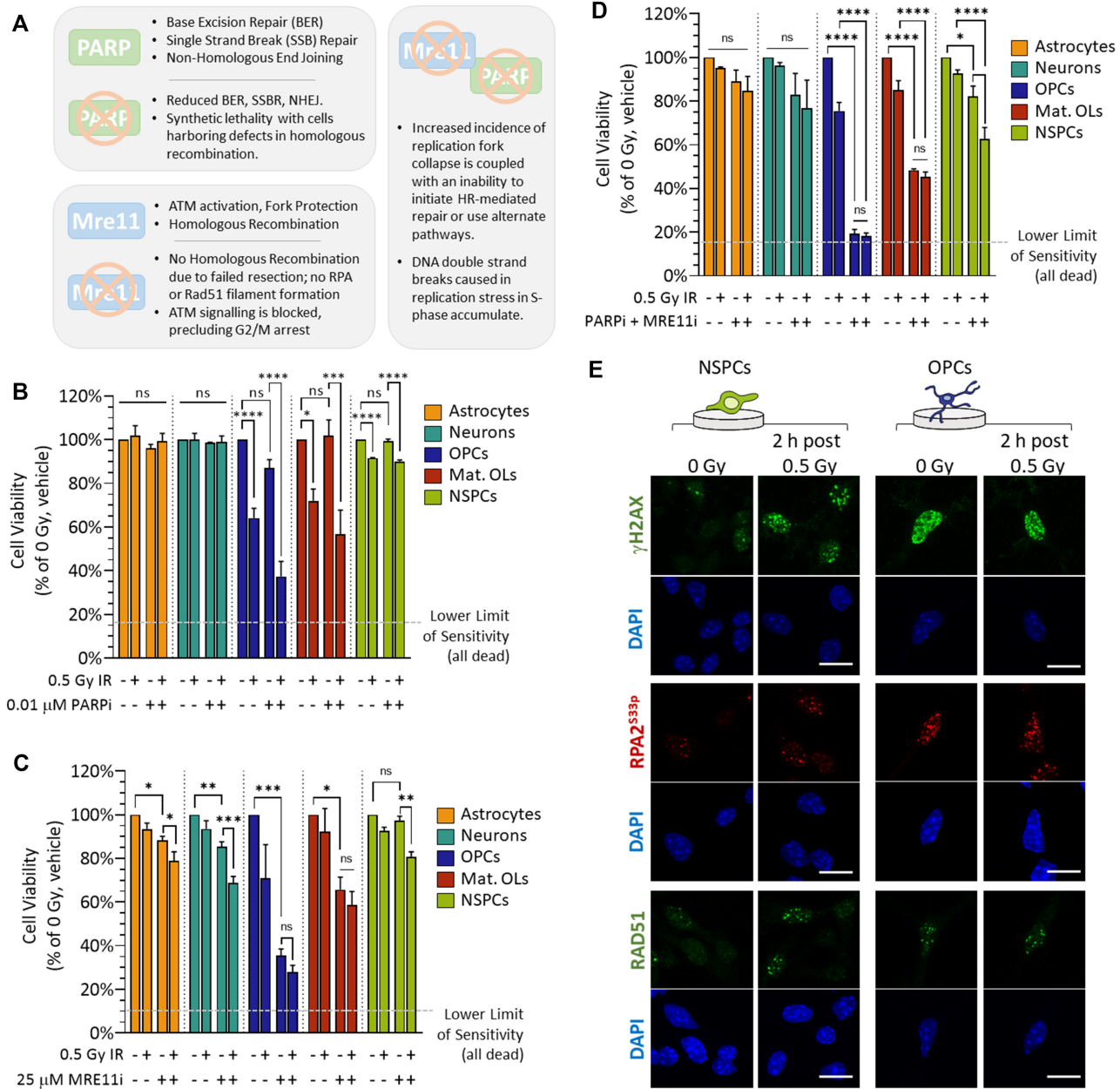
**Figure 5.** OPCs are highly reliant upon Mre11 nuclease-dependent pathways for survival, and show an IR-dependent lethality with PARP inhibitors. (**A**) A summary of the impact of PARP and/or MRE11 inhibition. (**B–D**) Individual neural cell lineages were treated with an equal amount of DMSO (vehicle) or 0.01 μM of the PARP inhibitor AZD-2281 (olaparib) (B), 25 μM of the Mre11 inhibitor Mirin (C), or both PARPi and Mre11i together (D) for 1 h, then exposed to 0.5 Gy IR and monitored 40 h later for viability using microplate reader. Bars represent mean ± SEM of $n = 3$ normalized to unirradiated, DMSO control. Data were analyzed with one-way ANOVAs amongst each neural cell type, and a Dunnett's multiple comparisons post-test compared each mean to the unirradiated, untreated control values. For panels B–D, ns $P > 0.05$, *$P < 0.05$, **$P < 0.01$, *** $P < 0.001$ and ****$P < 0.0001$, while ashed grey lines and skull icon represents the specific lower limit of sensitivity for this Alamar Blue assay (the point at which all cells in the culture are dead). (**E**) Asynchronously growing cultures of NSPCs and OPCs were irradiated with 0.5 Gy IR and, 2 h later, were fixed and stained the indicated markers. Scale bars indicate 10 μm.

## OPCs carry a high burden of anti-oxidant insensitive but DNA replication-associated DNA damage, and are sensitive to elevated replication fork collapse

To explore whether OPC radiosensitivity and endogenous DNA damage involves S-phase specific processes, we pulsed asynchronously proliferative OPC and NSPC cultures with EdU for 1 h to demarcate cells undergoing active DNA replication. We then counterstained cells with γH2AX and used flow cytometry to measure total nuclear γH2AX fluorescence (Figure 4A) or microscopy to enumerate nuclear γH2AX foci (Figure 4B) in S phase (EdU⁺) cells, and $G_1/G_2$ phase (EdU⁻) cells. As expected, endogenous γH2AX signal was highest in S-phase for both cell types, as cells undergoing DNA replication experience low-level
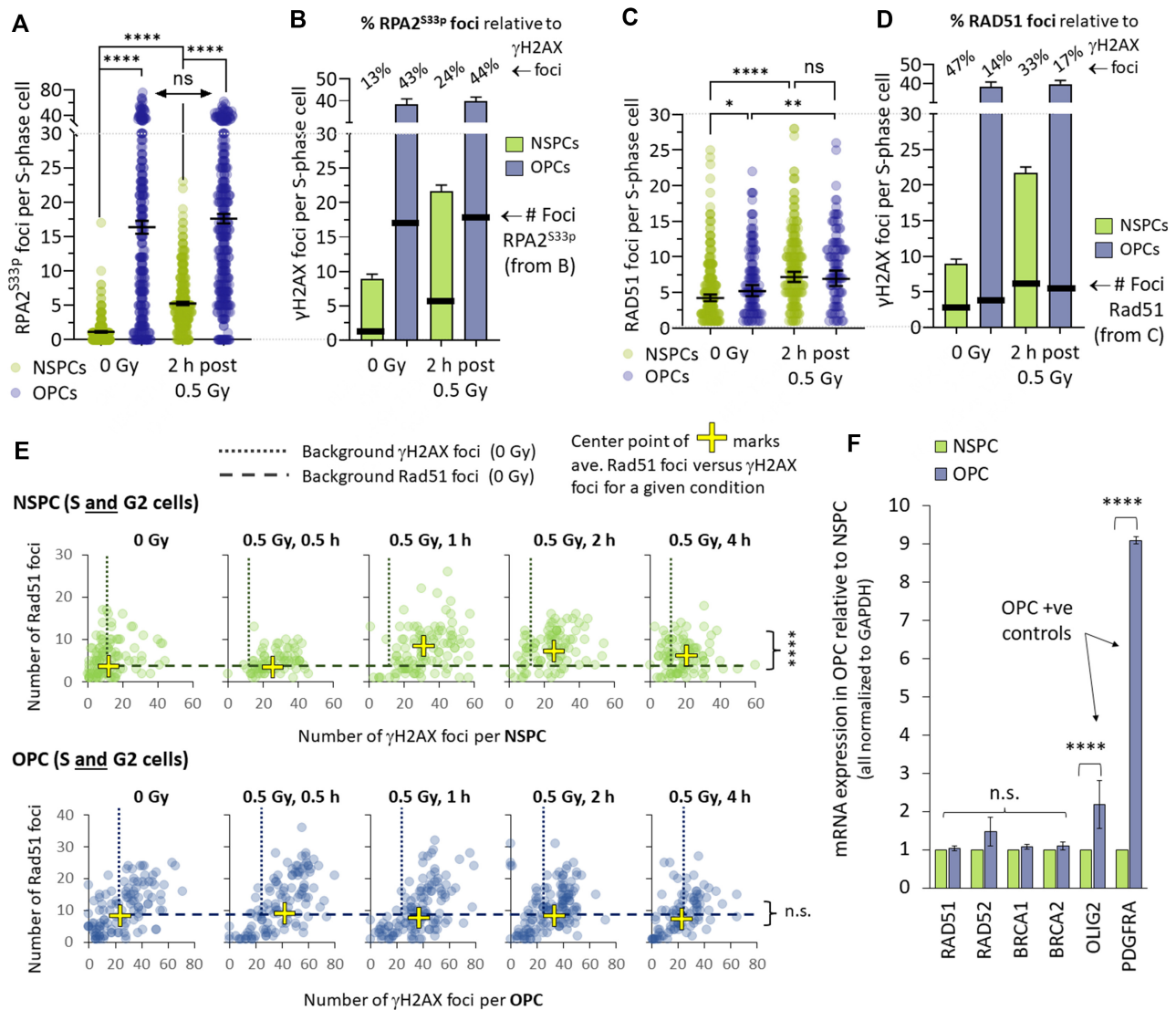
**Figure 6.** OPCs show normal RPA but insufficient RAD51 filament formation. (**A**) RPA2$^{S33p}$ foci were enumerated in S-phase cells from Figure 5E for between 65–85 cells per repeat ($n = 3$). G2-phase cells were excluded on the basis of positive signal for the G2/M-phase marker H3S10p. (**B**) The average γH2AX foci numbers from Figure 4B (green bars for NSPC, blue for OPC) were plotted relative to the mean number of RPA2$^{S33p}$ foci from (A). Percentage values at the top of each condition indicate the relative RPA2$^{S33p}$ foci to γH2AX foci. (**C**) Rad51 foci were enumerated in cells as in (A) for between 65 and 85 cells per repeat ($n = 3$). (**D**) The average γH2AX foci numbers from Figure 4B (green bars for NSPC, blue for OPC) were plotted relative to the mean number of Rad51 foci from (C). Percentage values at the top of each condition indicate the relative Rad51 foci to γH2AX foci. (**E**) Asynchronously growing OPC and NSPC cells were exposed to 0.5 Gy IR, harvested as indicated between 0.5–4 h later, and immunostained simultaneously for both γH2AX and RAD51 foci. OPC (blue dots) and NSPC (green dots) and enumerated for both γH2AX and RAD51 foci, which were expressed relative to one another over time. For each time point, yellow crosses represent the point of average γH2AX and RAD51 foci, while dashed lines are a reference point for the number of RAD51 in the unirradiated conditions, and dotted lines are the reference point for the number of γH2AX in the unirradiated condition. (**F**) qPCR analysis of the mRNA expression from the indicated genes was performed in unirradiated OPC and NSPC cultures, with all data normalized to the corresponding GAPDH value and expressed as fold change relative to expression in NSPC. All data represents $n = 3$ independent experiments. Statistical comparisons for all data are unpaired Student's $t$-tests. For all panels, ns $P > 0.05$, * $P < 0.05$, ** $P < 0.01$, *** $P < 0.001$ and **** $P < 0.0001$.

γH2AX due to mild ATR activation by RPA-coated lagging strands (51). However, S-phase OPCs showed a 2-fold greater γH2AX signal relative to the equally proliferative NSPC population, raising the possibility that OPCs may be uniquely and especially sensitive to replication stress. After verifying that antioxidants (still) had no impact OPCs in S phase (Figure 4C), similar to our previous observations with asynchronous OPC cultures (Figure 1G), we exposed cells to methyl methanesulfonate (MMS, methylates DNA

bases), or hydroxyurea (HU, depletes dNTPs) that will both stall DNA replication forks leading to an increased risk of collapse and 'one-ended' DSB formation requiring HR-mediated repair (60). Amongst the neural cell types, OPCs displayed the greatest sensitivity to MMS and HU (Figures 4D, E). In the context of pediatric brain tumor treatment, long term sequalae are also observed after etoposide, thiotepa or cisplatin chemotherapy, and all three produce DNA lesions that can collide with replication forks
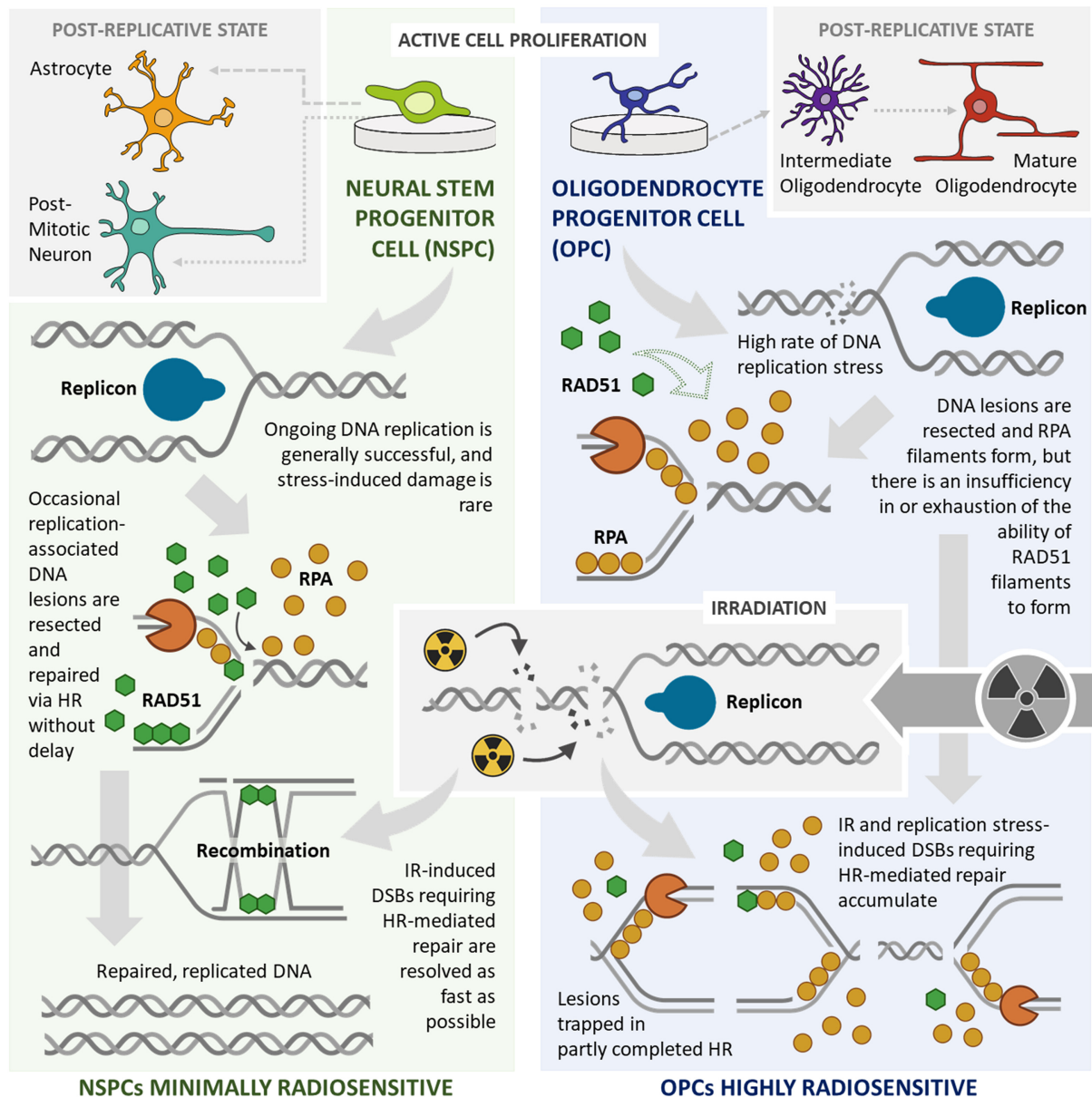
**Figure 7.** Model of the molecular mechanism of OPC radiosensitivity. (Left, green) DNA replication in NSPCs experiences low replications stress, and have sufficient RPA and RAD51-dependent homologous recombination (HR) DSB repair capacity to resolve collapsed forks successfully. Additional DNA damage incurred after irradiation is also repaired efficiently. (Right, blue) OPCs experience high rates of replication stress that interfere with DNA replication, but have limited RAD51 filament formation. RPA-coated, resected DSBs accumulate and cannot proceed through HR. Irradiation increases already high levels of collapsed replication forks, overwhelms insufficient OPC HR-mediated DSB repair capacity. Replication-associated DSBs accumulate in OPCs, leading to a higher degree of radiosensitivity relative to other cell types within the developing mammalian brain. This figure was created using Biorender.com and Microsoft PowerPoint.

to trigger collapse (60). We found that OPCs were also significantly more sensitive to etoposide, thiotepa or cisplatin treatment relative to NSPCs (Figure 4F), adding further credence to a putative DNA replication stress-centric model for OPC radiosensitivity.

**Mre11 inhibition is lethal to OPCs, while PARP inhibition synergizes with IR**

Elevated replication stress arises for multiple reasons, including innate defects in completing homology-mediated DSB repair (59,61). This condition is typically synthetic lethal with inhibition of poly (ADP-ribose) polymerase (PARP)-dependent repair pathways that are an alternate to HR (62–67). Cells with innate HR defects die characteristically in the presence of PARP inhibitors, whilst HR-competent cells are generally unaffected (Figure 5A). Elevated replication stress may also arise when HR-competent cells are pushed to an extreme by a burden of DNA damage that exceeds repair capacity at a given time, but may not be repairable by NHEJ-mediated DSB repair (e.g. 'one-ended' DSBs)(54,68). Lesions persist in this scenario, and

interfere with further replication fork progress; cells experiencing these conditions are typically sensitive to reductions in HR capacity, for example by MRE11 inhibition (69–71). To better define the nature of OPC replication stress, cells were incubated with inhibitors of PARP, MRE11 exonuclease activity, or both, at concentrations verified to produce known functional outcomes of specific enzyme activity loss (Supplementary Figure S4E, F), before being irradiated and monitored for viability (Figure 5B–D). PARP inhibition alone did not significantly ($P > 0.05$) impact astrocyte, neuron, NSPC, mOL or OPC viability (Figure 5B). PARP inhibition also had no impact on viability after IR in astrocytes, neurons, NSPCs or mOLs. In OPCs, however, PARPi significantly ($P < 0.0001$) exacerbated viability loss after IR, increasing death (in a greater than additive manner) from ∼40% (IR alone) to 63% (IR + PARPi). MRE11 inhibition alone reduced astrocyte, neuron and NSPC viability by ≤10%, and exacerbated IR effects to 20–25% death (Figure 5C). By contrast, the viability of OPCs and mOLs was reduced by 35–65% by MRE11 inhibitors alone, with no further impact by IR. For MRE11 inhibitor-treated astrocytes or neurons, PARPi had no added impact (with or without IR) (Figure 5D). PARPi and MRE11i effects were additive in NSPCs, reducing viability by 18%, and up to 38% after IR. Combined PARP and MRE11 inhibition significantly ($P < 0.0001$) reduced viability by 55% in mOLs and 82% in OPCs, with no further impacts produced by IR. In summary, the largest impacts on cell viability were observed in OPCs after PARPi + IR (63% loss), MRE11i ± IR (65–73% loss), and [MRE11 + PARPi] ± IR (81–82% loss). Other than intermediate effects in mOLs, all other neurological lineages were comparatively resistant to PARPi and MRE11i, similar to our findings with other DNA damage response inhibitors such as ATRi (Figure 3).

### OPCs complete RPA filament formation during HR-mediated DSB repair, but exhibit insufficiency in forming RAD51 foci

Our data suggest that OPCs are highly (and particularly) reliant on MRE11-dependent DSB repair pathways, and raise the possibility that OPCs harbor a modest but impactful HR 'insufficiency' that synergizes with PARP loss after IR. HR is initiated by 5′-3′ DSB end resection and subsequent formation of filaments of Replication Protein A (RPA), a heterotrimer of the which RPA2 is typically phosphorylated (e.g. RPA2 phosphoserine 33 (RPA2$^{S33p}$) in its filamentous form (56,59,72,73). Through the action of BRCA1 and other factors, RPA are exchanged for RAD51 filaments, which mediate DNA strand invasion and recombination to repair DSBs using an intact sister chromatid as a template (74,75). Limited HR capacity can arise from reduced DSB end resection (requiring MRE11) and/or a deficit in free RPA and/or RAD51 in situations where these proteins are: (i) under-expressed, (ii) filament formation factors are dysfunctional or (iii) there are so many 5′-3′ resected DSBs that all available RPA and/or RAD51 are sequestered into filaments (56,58,61). Once pools of free RPA and/or RAD51 are exhausted, already resected DSBs requiring HR-mediated repair 'have to wait', cannot be repaired by alternative pathways, and their persistence can reduce cell

viability. To investigate this, we monitored RPA2$^{S33p}$ and/or RAD51 foci numbers in NSPCs and OPCs in S-phase, relative to the total burden of DSBs demarcated by γH2AX foci (Figure 5E, 4A). The number of RPA2$^{S33p}$ foci generally reflected the observed relative burden of γH2AX foci in both cell types (Figure 6A, B). RPA2$^{S33p}$ foci were abundant in OPCs, representing 43% of persisting lesions, and were not significantly ($P > 0.05$) increased 2 h post 0.5 Gy IR. This data suggests that DSB end resection and RPA filament formation is operational in OPCs, but 'operating at' nearly maximum capacity even in resting cells. NSPCs carried a comparatively lower burden of RPA2$^{S33p}$ foci in unirradiated cells (13% of persisting lesions), but this doubled to 24% by 2 h post 0.5 Gy IR, also indicative of operational DSB resection. In NSPCs, RAD51 foci numbers reflected the RPA2$^{S33p}$ and γH2AX foci, being low in unirradiated cells, increasing after IR significantly ($P < 0.0001$), and being ∼35% of persisting lesions at any time. By contrast, RAD51 foci numbers in unirradiated OPCs was well below the number of RPA$^{S33p}$ foci, encompassed only 13% of persistent DSBs, and exposure to IR failed to increase this in a significant manner ($P > 0.05$) (Figure 6C, D).

Our data so far are indicative of a deficit in the ability of OPCs to enact Rad51-mediated HR relative to NSPCs, and is a plausible molecular explanation for radiosensitivity. To investigate this in greater detail, we enumerated both RAD51 and γH2AX foci in the same cells post 0.5 Gy IR over a 0.5 to 4 h time period (Figure 6E). This this case, S and G2 phase cells were scored together, as the combination of RAD51 and γH2AX foci precluded using markers used to exclude G2 phase. In both OPC and NSPCs, 0.5 Gy IR induced H2AX foci that peaked by 0.5–1 h and then decreased. In NSPCs, RAD51 foci increased significantly ($P < 0.0001$) after IR, peaked between 1–2 h, and then also decreased. As expected, unirradiated OPCs displayed a greater endogenous burden of H2AX foci; these increased and peaked 0.5 h after IR (similar to Figures 2D and 4B), and then decreased. However, the number of RAD51 foci in OPCs did not increase significantly ($P > 0.05$) above background at any time point after IR. To determine whether decreased transcription of RAD51 or the regulatory factors RAD52, BRCA1 or BRCA2 might contribute to this phenotype, we performed qPCR on NSPC and OPCs (Figure 6F). While positive controls (PDFGRA and OLIG2, as per Figure 1A) for the OPC lineage showed significant ($P < 0.0001$) greater transcripts in OPCs versus NSPCs, there was no significant ($P > 0.05$) difference in the expression of RAD51, RAD52, BRCA1 or BRCA2 between OPC and NSPCs. This eliminates reduced transcription of these key homologous recombination factors as being the underlying mechanism. Collectively, these experiments suggest that although OPC express RAD51, they experience significantly elevated endogenous DSBs that are directed towards HR-mediated repair processes that are confounded by a type of 'RAD51 exhaustion' wherein no further RAD51 foci are able to form after IR exposure.

### DISCUSSION

To summarize (Figure 7), we find that OPCs display an elevated burden of replication stress-associated DSBs need-

ing ATR and MRE11-dependent HR repair (Figures 2-5), they irreversibly commit to this repair pathway by successfully resecting DSBs to form RPA filaments (Figure 6A, B), but then encounter difficulties due to a reduced capacity to progress towards DNA strand invasion and recombination steps of HR that require RAD51 (Figure 6C–E). Consequently, replication-stress associated DSBs persist in OPCs, do not appear to be repaired by alternative means, and any incoming DSBs caused by IR have the potential to push cells towards death at lower doses relative to other neurological cell types (Figure 1B-C), while also generating an IR-specific PARPi sensitivity (Figure 5). As DNA-replication linked processes give rise to the elevated OPC burden of DNA damage needing HR, it makes mechanistic sense that maturation into a non-replicative mOL reduces sensitivity (Figures 1-5), chemotherapeutic agents that elevate replication stress exacerbate OPC death (Figures 4C–E), while suppression of oxidative stress using antioxidants has no major 'rescue effect' (Figure 1G and Supplementary Figure S4C).

Changes to brain white matter underlie a large proportion of the late effects of pediatric cranial radiotherapy. OPCs are the immature precursors of post-mitotic, myelinating oligodendrocytes that comprise most white matter, are present in high abundance in the early, developing brain, and the oligodendrocyte lineage have long been understood to be radiation sensitive (6,31–35). In this study, we have generated systematic cellular and molecular evidence for a new DNA damage and repair centric model for OPC radiosensitivity, arguing against the hypothesis that elevated oxidative stress is a major driver of the phenomenon. While elevated oxidative stress is a feature of OPC biology, that it can be suppressed without measurable impacts on OPC survival after IR indicates that an excess of reactive oxygen species is not causal to the elevated radiosensitivity. Instead, our data collectively suggest a model wherein OPCs carry a high replication stress-associated DNA damage burden that requires continual HR-mediated repair processes—a scenario that is prone to 'bottleneck' when challenged with radiation-induced DNA damage, due to limited available RAD51 needed to support the strand invasion and recombination steps HR to the same extent as other cell types also found in the brain. It is important to stress that we do not dispute that OPCs and other cells in the oligodendrocyte lineage experience high levels of oxidative stress—indeed, we also found this to be true. Oligodendrocyte lineage cells are rich in iron, low in antioxidants (such as glutathione), are highly metabolically active and are rich in oxidative radical-producing organelles (such as peroxisomes), all of which exacerbate ROS generation (11,30,76). Depletion of antioxidant precursors from oligodendrocytes impairs maturation, myelin formation and triggers apoptosis (77–79). Oligodendrocytes are highly sensitive to oxidative stress in models of hypoxic-ischemic injury (37,38,40,45,80), traumatic brain injuries (41,81), multiple sclerosis (43), and Alzheimer's disease (44). Indeed, reactive oxygen species in the oligodendrocyte lineage have been modulated by anti-oxidants for clinical gain in multiple disease models (20,40,45,46,80–87). In contrast to these successes, however, antioxidants have not shown clear benefit in animal models of brain irradiation examined over the past decade. These observations fit with our molecular data and, although OPC oxidative stress does respond robustly to short- and long-term antioxidant treatment, their failure to mitigate white matter changes and OPC loss supports our assertion that there is a distinct etiology for innate OPC radiosensitivity, namely replication stress.

Replication stress happens for a variety of reasons, including collisions between replication forks and alkylated bases, SSBs, DNA–protein adducts, DNA crosslinks, RNA:DNA hybrids and G-quadruplexes, or the perturbation of DNA polymerase progression (56,61,68). ATR has a critical role in suppressing the continuing firing of origins during replication stress to limit the amount of ss-DNA generated, and thus the amount of RPA needed to protect it (52,54,58,68). If the intra-S checkpoint is not activated by ATR, origins continue to fire as replication stress accumulates, RPA is exhausted, and forks collapse with increased frequency (55,58). Similarly, cellular pools of RAD51 become exhausted as BRCA1/2-dependent pathways exchange RPA for RAD51 filaments as part of HR-mediated DSB repair (75). As RAD51 filament-dependent HR events are slow by nature, eukaryotic cells display a limit in the net amount of HR that can take place at a given time, with any additional DSB repair requiring HR (i.e. resected and/or RPA-coated DSBs) being delayed until sufficient free RAD51 is made available (58,59,67). We suggest that our observations indicate a RAD51 filament formation exhaustion model for OPC radiosensitivity, where HR is operating at near capacity in the baseline, unirradiated state, and newly arising lesions *via* IR cannot productively undergo HR. This explains the innate sensitivity of the oligodendrocyte lineage to ATR inhibition but also MRE11 inhibition, as both are implicated in modulating fork speed and HR initiation in the event of fork collapse (53,57,69–71,74,88,89). This model may also explain why PARP inhibition had little impact on OPC viability alone, but its effects are greater than additive with IR as it 'forces' a larger proportion of IR-induced DSBs to be repaired via HR-mediated processes, which are already 'over-subscribed to' and unable to cope with increased DSB burdens. These results may also help mechanistically explain data showing that PARP inhibition has selective, slow cytotoxic effects on fetal tissue- but not adult tissue-derived OPCs from mice (90).

A key question that arises is what is the molecular basis for endogenous OPC replication stress? We postulate that this potentially could be due to an abundance of RNA:DNA hybrids (also called R-loops) that could arise from the specific transcription program of that phase of OPC physiology. R-loops are thermodynamically stable, three-stranded nucleic acid structures that form as nascent transcripts are produced by RNA polymerase, and are physiologically normal, regulate gene expression and DNA replication, but can cause DNA damage upon collision with replication machinery (91,92). While mRNA metabolism and RNase H-dependent processing processes R-loops in most cells, it is possible that the developmental and transcriptional context of an OPC results in the accumulation

of these R-loops thus producing innately high replicative stress.

The other important future direction is to address why OPCs are not able to support RAD51 filament formation to the same extent as NSPCs, especially given that RPA filament formation levels are comparable, as are transcription of the *RAD51, RAD52, BRCA1* and *BRCA2* genes (Figure 6F) that are RAD51-associated factors important for RAD51 function in DSB repair (93,94). To consolidate this work, it will be important to systematically monitor the mRNA and protein expression of all RAD51-regulatory factors in both the in vitro cell models used here, as well as in vivo mouse brains across early development. One challenge with this will be to obtain specific and sensitive antibodies that detect these factors in the mouse neurological context. Monitoring γH2AX foci in OPCs over time in developing mice is also a key experiment, albeit also technically challenging to achieve due to the logistics of anesthetization of early postnatal mice, subsequent tissue isolation, and cryopreservation in the timeframe relevant to DSB repair following acute IR exposure.

An interesting implication of this work relates to the etiology of secondary, radiotherapy-induced brain tumors, most often meningiomas and high-grade gliomas arising within the field of original radiation. These increase in incidence with IR or chemotherapy dose and the youth of the patient (9,15,17,95). OPCs are suspected as the cell of origin for malignant gliomas, which are characterized by PDGFRα gene amplifications and mutations and express high levels of OPC-specific markers such as Sox10, Nkx2.2, and Olig1/2 (8,21–23,25,26,95–98). Studies in B cell leukemia precursors have shown that highly transcribed lineage-specific genes such as Pax5 are prone to damage and mutations through direct transcription associated fragility, or interactions between replication and transcription machinery (99). It is possible that highly transcribed loci in OPCs (such as PDGFRα) accumulate DNA damage, leading to greater risk of amplification and/or activating mutations. In support of this, such alterations are observed in the genetic and molecular profiling of pediatric and young adult treatment-induced gliomas (8,22,26).

Finally, our data support the idea that OPCs have an inherent genomic instability that might predispose them to oncogenesis, particularly in the context of genotoxic insults at ages where OPCs are most abundant and proliferative. This fits with recent work profiling premalignant OPCs as likely sources of glioma, determining that *Nf1-Trp53* mutant OPCs within *in vivo* mouse models over-express HR-mediated DNA repair and nonsense-mediated decay markers, hypothesizing that transcription associated replication stress as a driver for gliomagenesis (100). Considering the sensitivity of OPCs to IR, we propose that perturbation of this sensitive cell type at an early age may underlie (at least in part) many of the late effects of pediatric cranial radiotherapy, including increased risk of cancer formation. Using this knowledge to develop interventions that better protect OPCs during radiotherapy merits further investigation, as it is needed to reduce the long-term negative impacts of this otherwise excellent treatment modality on childhood cancer survivors' lives.

## DATA AVAILABILITY

Raw datasets are available to researchers upon reasonable request to the corresponding authors.

## SUPPLEMENTARY DATA

Supplementary Data are available at NAR Cancer Online.

## REFERENCES

1. Acharya,S., Wu,S., Ashford,J.M., Tinkle,C.L., Lucas,J.T., Qaddoumi,I., Gajjar,A., Krasin,M.J., Conklin,H.M. and Merchant,T.E. (2019) Association between hippocampal dose and memory in survivors of childhood or adolescent low-grade glioma: a 10-year neurocognitive longitudinal study. *Neuro-oncol.*, **21**, 1175–1183.
2. Askins,M.A. and Moore,B.D. (2008) Preventing neurocognitive late effects in childhood cancer survivors. *J. Child Neurol.*, **23**, 1160–1171.
3. Beera,K.G., Li,Y.Q., Dazai,J., Stewart,J., Egan,S., Ahmed,M., Wong,C.S., Jaffray,D.A. and Nieman,B.J. (2018) Altered brain morphology after focal radiation reveals impact of off-target effects: Implications for white matter development and neurogenesis. *Neuro-oncol.*, **20**, 788–798.
4. Bledsoe,J.C. (2016) Effects of cranial radiation on structural and functional brain development in pediatric brain tumors. *J. Pediatr. Neuropsychol.*, **2**, 3–13.
5. Bloom,H.J.G., Wallace,E.N.K. and Henk,J.M. (1969) The treatment and prognosis of medulloblastoma in children. *Am. J. Roentgenol.*, **105**, 43–62.

6. Burns,T.C., Awad,A.J., Li,M.D. and Grant,G.A. (2016) Radiation-induced brain injury: low-hanging fruit for neuroregeneration. *Neurosurg. Focus*, **40**, 1–9.

7. De Ruiter,M.A., Van Mourik,R., Schouten-Van Meeteren,A.Y.N., Grootenhuis,M.A. and Oosterlaan,J. (2013) Neurocognitive consequences of a paediatric brain tumour and its treatment: A meta-analysis. *Dev. Med. Child Neurol.*, **55**, 408–417.

8. DeSisto,J., Lucas,J.T., Xu,K., Donson,A., Lin,T., Sanford,B., Wu,G., Tran,Q.T., Hedges,D., Hsu,C.-Y. *et al.* (2019) Comprehensive molecular characterization of pediatric radiation-induced high-grade glioma. *Nat. Commun.*, **12**, 5531.

9. Inskip,P.D., Sigurdson,A.J., Veiga,L., Bhatti,P., Ronckers,C., Rajaraman,P., Boukheris,H., Stovall,M., Smith,S., Hammond,S. *et al.* (2016) Radiation-related new primary solid cancers in the childhood cancer survivor study: Comparative radiation dose response and modification of treatment effects. *Int. J. Radiat. Oncol. Biol. Phys.*, **94**, 800–807.

10. Kantar,M., Çetingül,N., Kansoy,S., Anacak,Y., Demirtaş,E., Erşahin,Y. and Mutluer,S. (2004) Radiotherapy-induced secondary cranial neoplasms in children. *Child's Nervous Syst.*, **20**, 46–49.

11. McTigue,D.M. and Tripathi,R.B. (2008) The life, death, and replacement of oligodendrocytes in the adult CNS. *J. Neurochem.*, **107**, 1–19.

12. Moxon-Emre,I., Bouffet,E., Taylor,M.D., Laperriere,N., Sharpe,M.B., Laughlin,S., Bartels,U., Scantlebury,N., Law,N., Malkin,D. *et al.* (2016) Vulnerability of white matter to insult during childhood: Evidence from patients treated for medulloblastoma. *J. Neurosurg.: Pediatr.*, **18**, 29–40.

13. Mulhern,R.K., Merchant,T.E., Gajjar,A., Reddick,W.E. and Kun,L.E. (2004) Late neurocognitive sequelae in survivors of brain tumours in childhood. *Lancet Oncol.*, **5**, 399–408.

14. Mulhern,R.K., Reddick,W.E., Palmer,S.L., Glass,J.O., Elkin,T.D., Kun,L.E., Taylor,J., Langston,J. and Gajjar,A. (1999) Neurocognitive deficits in medulloblastoma survivors and white matter loss. *Ann. Neurol.*, **46**, 834–841.

15. Neglia,J.P., Robison,L.L., Stovall,M., Liu,Y., Packer,R.J., Hammond,S., Yasui,Y., Kasper,C.E., Mertens,A.C., Donaldson,S.S. *et al.* (2006) New primary neoplasms of the central nervous system in survivors of childhood cancer: A report from the childhood cancer survivor study. *J. Natl. Cancer Inst.*, **98**, 1528–1537.

16. Nieman,B.J., Elizabeth De Guzman,A., Gazdzinski,L.M., Lerch,J.P., Mallar Chakravarty,M., Pipitone,J., Strother,D., Fryer,C., Bouffet,E., Laughlin,S. *et al.* (2015) White and gray matter abnormalities after cranial radiation in children and mice. *Int. J. Radiat. Oncol. Biol. Phys.*, **93**, 882–891.

17. Relling,M.V., Rubnitz,J.E., Rivera,G.K., Boyett,J.M., Hancock,M.L., Felix,C.A., Kun,L.E., Walter,A.W., Evans,W.E. and Pui,C.H. (1999) High incidence of secondary brain tumours after radiotherapy and antimetabolites. *Lancet*, **354**, 34–39.

18. Ris,M.D., Packer,R., Goldwein,J., Jones-Wallace,D. and Boyett,J.M. (2001) Intellectual outcome after reduced-dose radiation therapy plus adjuvant chemotherapy for medulloblastoma: a Children's Cancer Group study. *J. Clin. Oncol.*, **19**, 3470–3476.

19. Robbins,M., Greene-Schloesser,D., Peiffer,A., Shaw,E., Chan,M. and Wheeler,K. (2012) Radiation-induced brain injury: a review. *Front. Oncol.*, **2**, 73–73.

20. Miyamoto,N., Maki,T., Pham,L.D.D., Hayakawa,K., Seo,J.H., Mandeville,E.T., Mandeville,J.B., Kim,K.W., Lo,E.H. and Arai,K. (2013) Oxidative stress interferes with white matter renewal after prolonged cerebral hypoperfusion in mice. *Stroke*, **44**, 3516–3521.

21. Azzarelli,R., Simons,B.D. and Philpott,A. (2018) The developmental origin of brain tumours: a cellular and molecular framework. *Development*, **145**, dev162693.

22. Donson,A.M., Erwin,N.S., Kleinschmidt-DeMasters,B.K., Madden,J.R., Addo-Yobo,S.O. and Foreman,N.K. (2007) Unique Molecular Characteristics of Radiation-Induced Glioblastoma. *J. Neuropathol. Exp. Neurol.*, **66**, 740–749.

23. Galvao,R.P., Kasina,A., McNeill,R.S., Harbin,J.E., Foreman,O., Verhaak,R.G.W., Nishiyama,A., Miller,C.R. and Zong,H. (2014) Transformation of quiescent adult oligodendrocyte precursor cells into malignant glioma through a multistep reactivation process. *Proc. Natl. Acad. Sci.*, **111**, E4214–E4223.

24. Ilkhanizadeh,S., Lau,J., Huang,M., Foster,D.J., Wong,R., Frantz,A., Wang,S., Weiss,W.A. and Persson,A.I. (2014) In:

25. Tew,K.D. and Fisher,P.B.B.T.A.i.C.R. (eds). Academic Press, Vol. **121**, pp. 1–65.

25. Liu,K.W., Hu,B. and Cheng,S.Y. (2011) Platelet-derived growth factor receptor alpha in Glioma: A bad seed. *Chin. J. Cancer*, **30**, 590–602.

26. López,G.Y., Van Ziffle,J., Onodera,C., Grenert,J.P., Yeh,I., Bastian,B.C., Clarke,J., Oberheim Bush,N.A., Taylor,J., Chang,S. *et al.* (2019) The genetic landscape of gliomas arising after therapeutic radiation. *Acta Neuropathol.*, **137**, 139–150.

27. Stiles,J. and Jernigan,T.L. (2010) The basics of brain development. *Neuropsychol. Rev.*, **20**, 327–348.

28. Gatz,S.A., Ju,L., Gruber,R., Hoffmann,E., Carr,A.M., Wang,Z.Q., Liu,C. and Jeggo,P.A. (2011) Requirement for DNA ligase IV during embryonic neuronal development. *J. Neurosci.*, **31**, 10088–10100.

29. Barazzuol,L. and Jeggo,P.A. (2016) In vivo sensitivity of the embryonic and adult neural stem cell compartments to low-dose radiation. *J Radiat Res*, **57**(Suppl. 1), i2–i10.

30. Baumann,N. and Pham-Dinh,D. (2001) Biology of oligodendrocyte and myelin in the mammalian central nervous system. *Physiol. Rev.*, **81**, 871–927.

31. Panagiotakos,G., Alshamy,G., Chan,B., Abrams,R., Greenberg,E., Saxena,A., Bradbury,M., Edgar,M., Gutin,P. and Tabar,V. (2007) Long-term impact of radiation on the stem cell and oligodendrocyte precursors in the brain. *PLoS One*, **2**, e588.

32. Begolly,S., Olschowka,J.A., Love,T., Williams,J.P. and O'Banion,M.K. (2018) Fractionation enhances acute oligodendrocyte progenitor cell radiation sensitivity and leads to long term depletion. *Glia*, **66**, 846–861.

33. Chow,B.M., Li,Y.Q. and Wong,C.S. (2000) Radiation-induced apoptosis in the adult central nervous system is p53-dependent. *Cell Death Differ.*, **7**, 712–720.

34. Li,Y.Q., Jay,V. and Wong,C.S. (1996) Oligodendrocytes in the adult rat spinal cord undergo radiation-induced apoptosis. *Cancer Res.*, **56**, 5417–5422.

35. Piao,J., Major,T., Auyeung,G., Policarpio,E., Menon,J., Droms,L., Gutin,P., Uryu,K., Tchieu,J., Soulet,D. *et al.* (2015) Human embryonic stem cell-derived oligodendrocyte progenitors remyelinate the brain and rescue behavioral deficits following radiation. *Cell Stem Cell*, **16**, 198–210.

36. Pearson,D.D., Anikin,A. and Goodarzi,A.A. (2016) In: I,K. and O,K. (eds). *Genome Stability*. Elsevier, pp. 712.

37. Chen,L.X., Ma,S.M., Zhang,P., Fan,Z.C., Xiong,M., Cheng,G.Q., Yang,Y., Qiu,Z.L., Zhou,W.H. and Li,J. (2015) Neuroprotective effects of oligodendrocyte progenitor cell transplantation in premature rat brain following hypoxic-ischemic injury. *PLoS One*, **10**, 1–16.

38. Falahati,S., Breu,M., Waickman,A.T., Phillips,A.W., Arauz,E.J., Snyder,S., Porambo,M., Goeral,K., Comi,A.M., Wilson,M.A. *et al.* (2013) Ischemia-induced neuroinflammation is associated with disrupted development of oligodendrocyte progenitors in a model of periventricular leukomalacia. *Dev. Neurosci.*, **35**, 182–196.

39. Georgiou,E., Sidiropoulou,K., Richter,J., Papaneophytou,C., Sargiannidou,I., Kagiava,A., Von Jonquieres,G., Christodoulou,C., Klugmann,M. and Kleopa,K.A. (2017) Gene therapy targeting oligodendrocytes provides therapeutic benefit in a leukodystrophy model. *Brain*, **140**, 599–616.

40. Itoh,K., Maki,T., Shindo,A., Egawa,N., Liang,A.C., Itoh,N., Lo,E.H., Lok,J. and Arai,K. (2016) Magnesium sulfate protects oligodendrocyte lineage cells in a rat cell-culture model of hypoxic-ischemic injury. *Neurosci. Res.*, **106**, 66–69.

41. Giacci,M.K., Bartlett,C.A., Smith,N.M., Iyer,K.S., Toomey,L.M., Jiang,H., Guagliardo,P., Kilburn,M.R. and Fitzgerald,M. (2018) Oligodendroglia are particularly vulnerable to oxidative damage after neurotrauma in vivo. *J. Neurosci.*, **38**, 6491–6504.

42. Cui,Q.L., Kuhlmann,T., Miron,V.E., Leong,S.Y., Fang,J., Gris,P., Kennedy,T.E., Almazan,G. and Antel,J. (2013) Oligodendrocyte progenitor cell susceptibility to injury in multiple sclerosis. *Am. J. Pathol.*, **183**, 516–525.

43. Neumann,B., Baror,R., Zhao,C., Segel,M., Dietmann,S., Rawji,K.S., Foerster,S., McClain,C.R., Chalut,K., van Wijngaarden,P. *et al.* (2019) Metformin restores CNS remyelination Capacity by rejuvenating aged stem cells. *Cell Stem Cell*, **25**, 473–485.

44. Nasrabady,S.E., Rizvi,B., Goldman,J.E. and Brickman,A.M. (2018) White matter changes in Alzheimer's disease: a focus on myelin and oligodendrocytes. *Acta Neuropathol. Commun.*, **6**, 22–22.

45. Takase,H., Liang,A.C., Miyamoto,N., Hamanaka,G., Ohtomo,R., Maki,T., Pham,L.D.D., Lok,J., Lo,E.H. and Arai,K. (2018) Protective effects of a radical scavenger edaravone on oligodendrocyte precursor cells against oxidative stress. *Neurosci. Lett.*, **668**, 120–125.

46. Kilanczyk,E., Ohri,S.S., Whittemore,S.R. and Hetman,M. (2016) Antioxidant protection of NADPH-depleted oligodendrocyte precursor cells is dependent on supply of reduced glutathione. *ASN Neuro*, **8**, 1759091416660404.

47. Chen,Y., Balasubramaniyan,V., Peng,J., Hurlock,E.C., Tallquist,M., Li,J. and Lu,Q.R. (2007) Isolation and culture of rat and mouse oligodendrocyte precursor cells. *Nat. Protoc.*, **2**, 1044–1051.

48. He,X., Li,Y., Lu,H., Zhang,Z., Wang,Y. and Yang,G.Y. (2013) Netrin-1 overexpression promotes white matter repairing and remodeling after focal cerebral ischemia in mice. *J. Cereb. Blood Flow Metab.*, **33**, 1921–1927.

49. Olszewska-Pazdrak,B., McVicar,S.D., Rayavara,K., Moya,S.M., Kantara,C., Gammarano,C., Olszewska,P., Fuller,G.M., Sower,L.E. and Carney,D.H. (2016) Nuclear countermeasure activity of TP508 linked to restoration of endothelial function and acceleration of DNA repair. *Radiat. Res.*, **186**, 162–174.

50. Moore,S., Berger,N.D., Luijsterburg,M.S., Piett,C.G., Stanley,F.K.T., Schrader,C.U., Fang,S., Chan,J.A., Schriemer,D.C., Nagel,Z.D. *et al.* (2019) The CHD6 chromatin remodeler is an oxidative DNA damage response factor. *Nat. Commun.*, **10**, 241.

51. Goodarzi,A.A. and Jeggo,P.A. (2012) Irradiation induced foci (IRIF) as a biomarker for radiosensitivity. *Mutat. Res.*, **736**, 39–47.

52. Ciccia,A. and Elledge,S.J. (2010) The DNA damage response: making it safe to play with knives. *Mol. Cell*, **40**, 179–204.

53. Couch,F.B., Bansbach,C.E., Driscoll,R., Luzwick,J.W., Glick,G.G., Bétous,R., Carroll,C.M., Jung,S.Y., Qin,J., Cimprich,K.A. *et al.* (2013) ATR phosphorylates SMARCAL1 to prevent replication fork collapse. *Genes Dev.*, **27**, 1610–1623.

54. Goodarzi,A.A. and Jeggo,P.A. (2013) The repair and signaling responses to DNA double-strand breaks. *Adv. Genet.*, **82**, 1–45.

55. Gupta,D., Lin,B., Cowan,A. and Heinen,C.D. (2018) ATR-Chk1 activation mitigates replication stress caused by mismatch repair-dependent processing of DNA damage. *Proc. Natl. Acad. Sci. U.S.A.*, **115**, 1523–1528.

56. Mehta,A. and Haber,J.E. (2014) Sources of DNA double-strand breaks and models of recombinational DNA repair. *Cold Spring Harb. Perspect. Biol.*, **6**, 1–17.

57. Saldivar,J.C., Hamperl,S., Bocek,M.J., Chung,M., Bass,T.E., Cisneros-Soberanis,F., Samejima,K., Xie,L., Paulson,J.R., Earnshaw,W.C. *et al.* (2018) An intrinsic S/G2 checkpoint enforced by ATR. *Science*, **361**, 806–810.

58. Toledo,L.I., Altmeyer,M., Rask,M.B., Lukas,C., Larsen,D.H., Povlsen,L.K., Bekker-Jensen,S., Mailand,N., Bartek,J. and Lukas,J. (2013) ATR prohibits replication catastrophe by preventing global exhaustion of RPA. *Cell*, **155**, 1088–1088.

59. Whelan,D.R., Lee,W.T.C., Yin,Y., Ofri,D.M., Bermudez-Hernandez,K., Keegan,S., Fenyo,D. and Rothenberg,E. (2018) Spatiotemporal dynamics of homologous recombination repair at single collapsed replication forks. *Nat. Commun.*, **9**, 895.

60. Vesela,E., Chroma,K., Turi,Z. and Mistrik,M. (2017) Common chemical inductors of replication stress: focus on cell-based studies. *Biomolecules*, **7**, 19.

61. Zeman,M.K. and Cimprich,K.A. (2014) Causes and consequences of replication stress. *Nat. Cell Biol.*, **16**, 2–9.

62. O'Connor,M.J. (2015) Targeting the DNA damage response in cancer. *Mol. Cell*, **60**, 547–560.

63. Hu,Y., Petit,S.A., Ficarro,S.B., Toomire,K.J., Xie,A., Lim,E., Cao,S.A., Park,E., Eck,M.J., Scully,R. *et al.* (2014) PARP1-driven poly-ADP-ribosylation regulates BRCA1 function in homologous recombination-mediated DNA repair. *Cancer Discov.*, **4**, 1430–1447.

64. Andrabi,S.A., Umanah,G.K., Chang,C., Stevens,D.A., Karuppagounder,S.S., Gagne,J.P., Poirier,G.G., Dawson,V.L. and Dawson,T.M. (2014) Poly(ADP-ribose) polymerase-dependent energy depletion occurs through inhibition of glycolysis. *Proc. Natl. Acad. Sci. U.S.A.*, **111**, 10209–10214.

65. Gibson,B.A. and Kraus,W.L. (2012) New insights into the molecular and cellular functions of poly(ADP-ribose) and PARPs. *Nat. Rev. Mol. Cell Biol.*, **13**, 411–424.

66. Chalmers,A.J., Lakshman,M., Chan,N. and Bristow,R.G. (2010) Poly(ADP-ribose) polymerase inhibition as a model for synthetic lethality in developing radiation oncology targets. *Semin. Radiat. Oncol.*, **20**, 274–281.

67. Helleday,T., Petermann,E., Lundin,C., Hodgson,B. and Sharma,R.A. (2008) DNA repair pathways as targets for cancer therapy. *Nat. Rev. Cancer*, **8**, 193–204.

68. Branzei,D. and Foiani,M. (2010) Maintaining genome stability at the replication fork. *Nat. Rev. Mol. Cell Biol.*, **11**, 208–219.

69. Olson,E., Nievera,C.J., Liu,E., Lee,A.Y.L., Chen,L. and Wu,X. (2007) The Mre11 Complex Mediates the S-Phase Checkpoint through an Interaction with Replication Protein A. *Mol. Cell. Biol.*, **27**, 6053–6067.

70. Petroni,M., Sardina,F., Infante,P., Bartolazzi,A., Locatelli,E., Fabretti,F., Di Giulio,S., Capalbo,C., Cardinali,B., Coppa,A. *et al.* (2018) MRE11 inhibition highlights a replication stress-dependent vulnerability of MYCN-driven tumors. *Cell Death Dis.*, **9**, 895.

71. Ying,S., Hamdy,F.C. and Helleday,T. (2012) Mre11-dependent degradation of stalled DNA replication forks is prevented by BRCA2 and PARP1. *Cancer Res.*, **72**, 2814–2821.

72. Shibata,A., Moiani,D., Arvai,A.S., Perry,J., Harding,S.M., Genois,M.M., Maity,R., van Rossum-Fikkert,S., Kertokalio,A., Romoli,F. *et al.* (2014) DNA double-strand break repair pathway choice is directed by distinct MRE11 nuclease activities. *Mol. Cell*, **53**, 7–18.

73. Jeggo,P.A., Pearl,L.H. and Carr,A.M. (2016) DNA repair, genome stability and cancer: a historical perspective. *Nat. Rev. Cancer*, **16**, 35–42.

74. Hashimoto,Y., Chaudhuri,A.R., Lopes,M. and Costanzo,V. (2010) Rad51 protects nascent DNA from Mre11-dependent degradation and promotes continuous DNA synthesis. *Nat. Struct. Mol. Biol.*, **17**, 1305–1311.

75. Mason,J.M., Chan,Y.L., Weichselbaum,R.W. and Bishop,D.K. (2019) Non-enzymatic roles of human RAD51 at stalled replication forks. *Nat. Commun.*, **10**.

76. Semple,B.D., Blomgren,K., Gimlin,K., Ferriero,D.M. and Noble-Haeusslein,L.J. (2013) Brain development in rodents and humans: Identifying benchmarks of maturation and vulnerability to injury across species. *Prog. Neurobiol.*, **106-107**, 1–16.

77. Back,S.A., Gan,X., Li,Y., Rosenberg,P.A. and Volpe,J.J. (1998) Maturation-dependent vulnerability of oligodendrocytes to oxidative stress-induced death caused by glutathione depletion. *J. Neurosci.*, **18**, 6241–6253.

78. Butts,B.D., Houde,C. and Mehmet,H. (2008) Maturation-dependent sensitivity of oligodendrocyte lineage cells to apoptosis: Implications for normal development and disease. *Cell Death Differ.*, **15**, 1178–1186.

79. Monin,A., Baumann,P.S., Griffa,A., Xin,L., Mekle,R., Fournier,M., Butticaz,C., Klaey,M., Cabungcal,J.H., Steullet,P. *et al.* (2015) Glutathione deficit impairs myelin maturation: Relevance for white matter integrity in schizophrenia patients. *Mol Psychiatr*, **20**, 827–838.

80. Park,D., Shin,K., Choi,E.K., Choi,Y., Jang,J.Y., Kim,J., Jeong,H.S., Lee,W., Lee,Y.B., Kim,S.U. *et al.* (2015) Protective effects of N-acetyl-L-cysteine in human oligodendrocyte progenitor cells and restoration of motor function in neonatal rats with hypoxic-ischemic encephalopathy. *Evid.-Based Complement. Altern. Med.*, **2015**, 764251.

81. Haber,M., James,J., Kim,J., Sangobowale,M., Irizarry,R., Ho,J., Nikulina,E., Grin'kina,N.M., Ramadani,A., Hartman,I. *et al.* (2018) Minocycline plus N-acteylcysteine induces remyelination, synergistically protects oligodendrocytes and modifies neuroinflammation in a rat model of mild traumatic brain injury. *J. Cereb. Blood Flow Metab.*, **38**, 1312–1326.

82. Eleuteri,C., Olla,S., Veroni,C., Umeton,R., Mechelli,R., Romano,S., Buscarinu,M.C., Ferrari,F., Calò,G., Ristori,G. *et al.* (2017) A staged screening of registered drugs highlights remyelinating drug candidates for clinical trials. *Sci. Rep.*, **7**, 1–15.

83. Kubo,K., Nakao,S., Jomura,S., Sakamoto,S., Miyamoto,E., Xu,Y., Tomimoto,H., Inada,T. and Shingu,K. (2009) Edaravone, a free

radical scavenger, mitigates both gray and white matter damages after global cerebral ischemia in rats. *Brain Res.*, **1279**, 139–146.

84. Perfeito,R., Pereira,J., Oliveira,C., Bettencourt-Relvas,J. and Rego,A.C. (2007) Trolox protection of myelin membrane in hydrogen peroxide-treated mature oligodendrocytes. *Free Rad. Res.*, **41**, 444–451.

85. Takei,K., Watanabe,K., Yuki,S., Akimoto,M., Sakata,T. and Palumbo,J. (2017) Edaravone and its clinical development for amyotrophic lateral sclerosis. *Amyotrop. Lateral Scl. Frontotemporal Degener.*, **18**, 5–10.

86. Ueno,Y., Zhang,N., Miyamoto,N., Tanaka,R., Hattori,N. and Urabe,T. (2009) Edaravone attenuates white matter lesions through endothelial protection in a rat chronic hypoperfusion model. *Neuroscience*, **162**, 317–327.

87. Wu,S., Sena,E., Egan,K., Macleod,M. and Mead,G. (2014) Edaravone improves functional and structural outcomes in animal models of focal cerebral ischemia: A systematic review. *Int. J. Stroke*, **9**, 101–106.

88. Kim,H.S., Nickoloff,J.A., Wu,Y., Williamson,E.A., Sidhu,G.S., Reinert,B.L., Jaiswal,A.S., Srinivasan,G., Patel,B., Kong,K. *et al.* (2017) Endonuclease EEPD1 Is a gatekeeper for repair of stressed replication forks. *J. Biol. Chem.*, **292**, 2795–2804.

89. Schlacher,K., Christ,N., Siaud,N., Egashira,A., Wu,H. and Jasin,M. (2011) Double-strand break repair-independent role for BRCA2 in blocking stalled replication fork degradation by MRE11. *Cell*, **145**, 529–542.

90. Baldassarro,V.A., Marchesini,A., Giardino,L. and Calza,L. (2017) PARP activity and inhibition in fetal and adult oligodendrocyte precursor cells: Effect on cell survival and differentiation. *Stem Cell Res*, **22**, 54–60.

91. Allison,D.F. and Wang,G.G. (2019) R-loops: formation, function, and relevance to cell stress. *Cell Stress*, **3**, 38–46.

92. Sollier,J. and Cimprich,K.A. (2015) Breaking bad: R-loops and genome integrity. *Trends Cell Biol.*, **25**, 514–522.

93. Matos-Rodrigues,G., Guirouilh-Barbat,J., Martini,E. and Lopez,BS. (2021) Homologous recombination, cancer and the 'RAD51 paradox'. *NAR Cancer*, **3**, zcab016.

94. Penninckx,S., Pariset,E., Cekanaviciute,E. and Costes,S.V. (2021) Quantification of radiation-induced DNA double strand break repair foci to evaluate and predict biological responses to ionizing radiation. *NAR Cancer*, **3**, zcab046.

95. Puget,S., Philippe,C., Bax,D.A., Job,B., Varlet,P., Junier,M.P., Andreiuolo,F., Carvalho,D., Reis,R., Guerrini-Rousseau,L. *et al.* (2012) Mesenchymal transition and pdgfra amplification/mutation are key distinct oncogenic events in pediatric diffuse intrinsic pontine gliomas. *PLoS One*, 7.

96. Bohm,A.K., DePetro,J., Binding,C.E., Gerber,A., Chahley,N., Berger,N.D., Ware,M., Thomas,K., Senapathi,U., Bukhari,S. *et al.* (2020) In vitro modeling of glioblastoma initiation using PDGF-AA and p53-null neural progenitors. *Neuro-oncol.*, **22**, 1150–1161.

97. Fortin,J., Tian,R., Zarrabi,I., Hill,G., Williams,E., Sanchez-Duffhues,G., Thorikay,M., Ramachandran,P., Siddaway,R., Wong,J.F. *et al.* (2020) Mutant ACVR1 arrests glial cell differentiation to drive tumorigenesis in pediatric gliomas. *Cancer Cell*, **37**, 308–323.

98. Persson,A.I., Petritsch,C., Swartling,F.J., Itsara,M., Sim,F.J., Auvergne,R., Goldenberg,D.D., Vandenberg,S.R., Nguyen,K.N., Yakovenko,S. *et al.* (2010) Non-stem cell origin for oligodendroglioma. *Cancer Cell*, **18**, 669–682.

99. Boulianne,B., Robinson,M.E., May,P.C., Castellano,L., Blighe,K., Thomas,J., Reid,A., Müschen,M., Apperley,J.F., Stebbing,J. *et al.* (2017) Lineage-specific genes are prominent DNA damage hotspots during leukemic transformation of B cell precursors. *Cell Rep.*, **18**, 1687–1698.

100. Sutcliffe,M.D., Galvao,R.P., Wang,L., Kim,J., Rosenfeld,L.K., Singh,S., Zong,H. and Janes,K.A. (2021) Premalignant oligodendrocyte precursor cells stall in a heterogeneous state of replication stress prior to hliomagenesis. *Cancer Res.*, **81**, 1868–1882.